

# Probing evolution of binaries influenced by the spin-orbit resonances

A Gupta<sup>1</sup> & A Gopakumar<sup>1</sup>

<sup>1</sup> Department of Astronomy and Astrophysics, Tata Institute of Fundamental Research, Mumbai 400005, India

E-mail: [arg@tifr.res.in](mailto:arg@tifr.res.in), [gopu@tifr.res.in](mailto:gopu@tifr.res.in)

## Abstract.

We evolve isolated comparable mass spinning compact binaries experiencing Schnittman's post-Newtonian spin-orbit resonances in an inertial frame associated with  $\mathbf{j}_0$ , the initial direction of the total angular momentum. We argue that accurate gravitational wave (GW) measurements of the initial orientations of the two spins and orbital angular momentum from  $\mathbf{j}_0$  should allow us to distinguish between the two possible families of spin-orbit resonances. Therefore, these measurements have the potential to provide direct observational evidence of possible binary formation scenarios. The above statements should also apply for binaries that do not remain in a resonant plane when they become detectable by GW interferometers. The resonant plane, characterized by the vanishing scalar triple product involving the two spins and the orbital angular momentum, naturally appears in the one parameter family of equilibrium solutions, discovered by Schnittman. We develop a prescription to compute the time-domain inspiral templates for binaries residing in these resonant configurations and explore their preliminary data analysis consequences.

PACS numbers: 04.25.Nx, 04.30.-w, 97.60.Lf, 95.30.Sf

Submitted to: *Class. Quantum Grav.*

## 1. Introduction

Coalescing comparable mass compact binaries containing spinning stellar mass black holes (BHs) are among the expected gravitational wave (GW) sources for the ground based interferometric GW detectors like advanced LIGO (aLIGO), advanced Virgo and KAGRA [1]. In comparison, comparable mass spinning supermassive BH binaries will be required to realize GW astronomy in the milli-Hertz and nano-Hertz regimes in the coming decades [2, 3]. The optimal data analysis method of *matched filtering* is being invoked to extract the weak GW signals that are deeply buried in the noisy data sets. In this method one cross-correlates the relevant data with several template banks that contain accurately modeled GW signals from a number of expected compact binary sources. The construction of these GW search templates requires one to model GW polarization states,  $h_{\times}(t)$  and  $h_{+}(t)$ , associated with the inspiral phase of coalescing compact binaries in an accurate and efficient manner. Fortunately, GWs emitted during the inspiral phase can be accurately modeled by invoking the post-Newtonian

(PN) approximation to general relativity. In the case of non-spinning compact binaries, inspiraling along quasi-circular orbits, theoretical inputs required to compute highly accurate inspiral phase templates are available to the 3.5PN order. These include inputs to compute the fully 3.5PN accurate orbital phase evolution and 3PN accurate expressions for  $h_{\times}(t)$  and  $h_{+}(t)$  [4, 5, 6]. Recall that  $n$ PN corrections provide contributions that are accurate to the relative  $(v/c)^{2n}$  order beyond the Newtonian estimate, where  $v$  and  $c$  are the orbital and light speeds, respectively. Interestingly, there are on-going efforts to describe the compact binary dynamics at the conservative 4PN order [7]. In the case of binaries containing Kerr BHs, the spin effects should be incorporated while constructing appropriate search templates. This is the main motivation for the ongoing efforts to compute the higher PN order corrections to the dominant order spin-orbit and spin-spin contributions to the dynamics of spinning compact binaries, computed some four decades ago by Barker and O’Connell [8]. We observe that for compact binaries, containing maximally spinning BHs, the leading order spin-orbit and spin-spin interactions enter the orbital dynamics at 1.5PN and 2PN order, respectively [9]. At present, the next-to-next-to-leading order spin-orbit contributions that appear at 3.5PN order are available in [10] while the next-to-next-to-leading order spin-orbit and spin(1)-spin(2) Hamiltonians are available in [11]. Very recently, the next-to-next-to-leading order spin-orbit contributions to the gravitational wave flux and associated orbital phase evolutions were obtained for binaries in quasi-circular orbits [12]. Strictly speaking, we only have all the relevant inputs to perform GW phasing to 2.5PN order while incorporating all the spin effects associated with the two maximally spinning Kerr BHs. In comparison, the ready-to-use amplitude corrected GW polarization states are only available to 2PN order for binaries in quasi-circular orbits [13, 14, 15] and to 1PN order for eccentric binaries [16]. In what follows, we explore the evolution of certain binary configurations that contain two spinning compact objects of comparable masses  $m_1$  and  $m_2$  ( $m_1 \gtrsim m_2$ ) and having Kerr parameters  $\chi_1$  and  $\chi_2$  such that their spin angular momenta are given by  $\mathbf{S}_1 = G m_1^2 \chi_1 \mathbf{s}_1/c$  and  $\mathbf{S}_2 = G m_2^2 \chi_2 \mathbf{s}_2/c$ .

Roughly a decade ago, Schnittman discovered certain equilibrium configurations for spinning and precessing compact binaries [17]. The binaries in such configurations have their two spins and the orbital angular momentum  $\mathbf{L}$  lying in the same plane and the definition of the total angular momentum, namely  $\mathbf{J} = \mathbf{L} + \mathbf{S}_1 + \mathbf{S}_2$ , implies that  $\mathbf{J}$  will also lie in this plane. Schnittman observed that spinning compact binaries in these equilibrium configurations are characterized by constant values of  $\mathbf{s}_1 \cdot \mathbf{s}_2$ ,  $\mathbf{k} \cdot \mathbf{s}_1$  and  $\mathbf{k} \cdot \mathbf{s}_2$  during the precessional time scale, where  $\mathbf{s}_1$ ,  $\mathbf{s}_2$  and  $\mathbf{k}$  are unit vectors along the two spins and orbital angular momenta, respectively. Schnittman termed these equilibrium solutions as the “spin-orbit resonant configurations” as  $\mathbf{s}_1$ ,  $\mathbf{s}_2$  and  $\mathbf{L}$  precess around  $\mathbf{J}$  with a constant frequency for such binaries in the absence of gravitational radiation reaction effects ( $\mathbf{J}$  is a conserved quantity both in magnitude and direction in the absence of GW damping). With the inclusion of the reactive contributions in PN-accurate orbital dynamics, Schnittman observed that  $\mathbf{s}_1 \cdot \mathbf{s}_2$  approaches unity on the inspiral timescale for certain type of equilibrium configurations. Therefore, the equilibrium configurations experience the spin alignment towards the end of their inspiral. Binaries, not initially in the neighborhood of these equilibrium configurations, can eventually get locked and librate around them during their inspiral. The spin-orbit resonances may have important astrophysical implications as noted in [17, 18, 19, 20]. This is because of the ability of these resonances to align the spins of comparable mass supermassive BH binaries prior to their mergers [18, 20]. This will ensure

that the massive BHs formed via BH coalescences will not experience large recoil velocities. Therefore, the merger remnants may be retained in their host galaxies that are hierarchically formed from the merger of smaller galaxies. Very recently, it was argued that the BH spins in comparable mass stellar mass BH binaries would lie preferentially in a resonant plane due the spin-orbit resonances when their GWs enter the aLIGO frequency window [19]. They demonstrated that PN evolution forces the two spins to lie in certain resonant planes, characterized by either  $\Delta\tilde{\phi} = \pm 180^\circ$  or  $\Delta\tilde{\phi} = 0^\circ$  where  $\Delta\tilde{\phi}$  is the relative angular separation between the two spins in an associated orbital plane (this requires that the tides are efficient during the formation of these binaries). The binaries belonging to these two  $\Delta\tilde{\phi}$  families are forced to belong to what they termed as the standard mass ratio (SMR) and the reverse mass ratio (RMR) binary formation scenarios. In the SMR binary formation channel, the more massive star will evolve to form the more massive component of the BH binary and the compact binary during its inspiral will be influenced by the  $\Delta\tilde{\phi} = \pm 180^\circ$  spin-orbit resonances. In contrast, the heavier BH forms during the second supernova explosion in the RMR binary formation scenario and this is essentially due to the substantial mass transfer during the Roche lobe overflow of the progenitor. Such BH binaries are expected to get influenced by the  $\Delta\tilde{\phi} = 0^\circ$  resonances. Gerosa *et. al* studied in detail the combined effects of efficient tides and supernova kicks (both isotropic and polar) on the above two binary formation channels. Their detailed explorations allowed them to provide several distributions for the misalignments between  $\mathbf{k}$  and the two spins at orbital separations of roughly 500 Schwarzschild radius (see the  $a = 1000 M$  scatter plots in figures 5 and 6 in [19]). These scatter plots turned out to be very helpful in providing the initial conditions for our numerical investigations. Gerosa *et. al* also explored the binary formation scenarios involving inefficient tides and termed the resulting binaries as the freely precessing ones. It was pointed out that the accurate matched filtering measurements of  $\Delta\tilde{\phi}$  and  $\theta_{12} = \cos^{-1}(\mathbf{s}_1 \cdot \mathbf{s}_2)$  from a large sample of GW observations will constrain the various possible models of binary formation [19]. We note that it is customary to probe the dynamics of these inspiraling and precessing binaries in an orbital triad associated with the Newtonian orbital angular momentum  $\mathbf{L}_N = \mu \mathbf{r} \times \mathbf{v}$ , where  $\mu$ ,  $\mathbf{r}$  and  $\mathbf{v}$  are the reduced mass, orbital separation and velocity, respectively.

In this paper, we evolve comparable mass spinning compact binaries from an initial epoch characterized by  $x = 10^{-3}$  (we usually denote this specific  $x$  value as  $x_i$ ). The dimensionless PN expansion parameter  $x$  is defined in terms of an orbital-like frequency  $\omega$  and the total mass  $m$ :  $x \equiv (Gm\omega/c^3)^{2/3}$ . We use the orbital angular momentum  $\mathbf{L}$  rather than its Newtonian counterpart  $\mathbf{L}_N$  to describe the binary orbits. Additionally, we invoke an inertial frame associated with  $\mathbf{j}_0$ , the unit vector along the initial direction of the total angular momentum of the binary, to specify both the orbital and spin angular momenta. In contrast, it is common to invoke an  $\mathbf{L}_N$ -based non-inertial triad to specify the two spins at the initial epoch. We observe that is customary to numerically evolve  $\mathbf{L}_N$  by invoking the precessional equation appropriate for  $\mathbf{L}$  while incorporating the effects of dominant order spin-orbit coupling [15]. The initial  $x$  value makes sure that these compact binaries inspiral essentially due to the emission of GWs from orbital separations  $\sim 500 R_s$  where  $R_s \equiv 2Gm/c^2$  being the Schwarzschild radius. We terminate these numerical integrations when  $x$  reaches either of the following two fiducial values:  $x = x_0$  or  $x = x_f \equiv 0.1$ . In our numerical integrations,  $x_0 \equiv (Gm\omega_0/c^3)^{2/3}$  where  $\omega_0 \sim 10\pi$  Hz for ground-based interferometers like aLIGO while  $\omega_0 \sim 10^{-4}\pi$  Hz for eLISA. The  $x_f$  value is

essentially influenced by the earlier investigations [17, 18]. We evolve comparable mass spinning compact binaries that satisfy the set of equilibrium spin configurations at  $x_i$ , discovered by Schnittman. These one parameter family of equilibrium configurations, characterized either by  $\Delta\phi = 0^\circ$  or  $\pm 180^\circ$ , can be obtained by demanding that both  $\gamma \equiv [\mathbf{k}, \mathbf{s}_1, \mathbf{s}_2] = \mathbf{k} \cdot (\mathbf{s}_1 \times \mathbf{s}_2)$  and its time derivative should vanish at the initial epoch [17]. In our approach,  $\Delta\phi$  provides the relative angular separation of the two spins in a plane perpendicular to  $\mathbf{j}_0$ . Recall that these equilibrium configurations may be viewed as spin-orbit resonances as the precession frequencies of  $\mathbf{L}$ ,  $\mathbf{s}_1$  and  $\mathbf{s}_2$  around  $\mathbf{j}_0$  are rather identical. We argue that accurate matched filtering measurements of the orientations of  $\mathbf{s}_1$ ,  $\mathbf{s}_2$  and  $\mathbf{k}$  from  $\mathbf{j}_0$  at  $x_0$  should allow us to distinguish between binaries under the influence of either  $\Delta\phi = 0^\circ$  or  $\Delta\phi = \pm 180^\circ$  spin-orbit resonances. Therefore, these accurate GW measurements from an inspiraling comparable mass spinning binary should provide, in principle, the direct observational evidence of binary formation channels involving the SMR or RMR scenarios that also involve efficient tides, as detailed in [19]. To illustrate the above statement, let  $\theta'_1, \theta'_2$  and  $\iota'$  stand for the orientations of  $\mathbf{s}_1, \mathbf{s}_2$  and  $\mathbf{k}$  from  $\mathbf{j}_0$  at  $x_0$ . We show that the binaries that are influenced by  $\Delta\phi = \pm 180^\circ$  resonances tend to have  $\theta'_1 > \theta'_2 > \iota'$ . The typical  $\iota'$  values are usually lie below  $10^\circ$ . However, negligible  $\iota'$  values suggest very efficient tides during the binary formation. In contrast,  $\Delta\phi = 0^\circ$  resonant binaries tend to have  $\theta'_2 > \theta'_1 > \iota'$  and typical  $\iota'$  values are  $> 10^\circ$ . Non-negligible  $\iota'$  values in the range of few degrees indicate efficient tides during the binary formation. We show that the above inferences also apply for binaries that do not remain in a resonant plane when they become detectable by GW interferometers. The resonant plane, characterized by either  $\Delta\phi = 0^\circ$  or  $\Delta\phi = \pm 180^\circ$  restrictions, naturally appears in the above mentioned one parameter family of equilibrium solutions.

It turns out that the two black hole spins and the orbital angular momentum do not remain in a plane during the late stages of inspiral for binaries that were not in Schnittman's equilibrium configurations at  $x_i$ . Indeed, these binaries are influenced by the spin-orbit resonances and get locked into a nearby resonant plane during their inspiral. However, this may not be sufficient to force the above three vectors to share a common plane when these binaries inspiral to  $x_0$ . For such binaries, the above listed angular variables librate around their resonant values and the plots for  $\Delta\phi(x)$  and  $\gamma(x)$  can have non-negligible amplitudes during the late stages of inspiral. We also emphasize the importance of measuring accurately the values of  $\theta_{12}$  at  $x_0$ . The accurate  $\theta_{12}(x_0)$  measurements turned out to be crucial to distinguish the freely precessing binaries from those under the influence of the spin-orbit resonances. Following Gerosa *et. al*, the freely precessing binaries are expected to have  $\theta_1(x_i) \sim \theta_2(x_i)$  as the tidal interactions play no significant role during their formation. Additionally, such binaries are not affected by the spin-orbit resonances during their inspiral from  $x_i$  to  $x_0$  [19]. Our numerical integrations show that these binaries can mimic the constraints on the  $\theta'_1, \theta'_2$  and  $\iota'$  values that are satisfied by the two resonant families. However, the  $\theta_{12}(x_0)$  values of freely precessing binaries will not obey two specific relations, involving  $\theta'_1$  and  $\theta'_2$  values, that are fulfilled by binaries affected by the spin-orbit resonances. This is relevant as binaries under the influence of  $\Delta\phi = 0^\circ$  ( $\Delta\phi = \pm 180^\circ$ ) spin-orbit resonances are expected to have  $\theta_{12}(x_0) \sim \theta'_2 - \theta'_1$  ( $\theta_{12}(x_0) \sim \theta'_1 + \theta'_2$ ). Therefore, the accurate measurements of  $\theta'_1, \theta'_2, \iota'$  and  $\theta_{12}(x_0)$  values are crucial to distinguish the three possible types of inspiraling comparable mass spinning binaries. These three possible types, as expected, include binaries that are either freely precessing or influenced by one of the two spin-orbit resonances (the

$\Delta\phi = 0$  or  $\Delta\phi = \pm 180^\circ$  resonances).

We also develop a prescription to compute the time domain GW polarization states for comparable mass spinning compact binaries experiencing spin-orbit resonances in the aLIGO/eLISA frequency windows. Our approach invokes  $\mathbf{k}$  to describe the binary orbits and the  $\mathbf{j}_0$ -based inertial frame to specify the two spins and is based on [15]. Therefore, our approach can easily incorporate various expressions that are required to analyze the spin-orbit resonances in a  $\mathbf{j}_0$ -based inertial frame. We show that the temporally evolving  $h_{\times,+}(t)$  are uniquely characterized by only six parameters at the fiducial  $x_0$  values for binaries that reside in the resonant planes. These six parameters include the four basic ones, namely  $m$ ,  $\eta(= m_1 m_2/m^2)$ ,  $\chi_1$ ,  $\chi_2$  and the two angular parameters,  $\theta_1(x_0)$  and  $\phi_1(x_0)$ , that specify the orientation of more massive spin at  $x_0$ . The requirement that  $\gamma$  and its time derivative should be zero at  $x_0$  forces the orientation of  $\mathbf{s}_2$  to become dependent parameters for such binaries. In comparison, one requires to specify eight parameters to obtain  $h_{\times,+}(t)$  for binaries not residing in the resonant plane. This is essentially due to the non-vanishing  $\gamma$  and  $\dot{\gamma}$  values at  $x_0$  for such binaries. Invoking the match  $\mathcal{M}$  computations, detailed in [21], we compare inspiral templates for binaries residing in and librating around the resonant configurations in aLIGO frequency window. Binaries in ‘near-resonance’ configurations tend to have  $\mathcal{M}$  estimates  $> 0.9$  while the  $\mathcal{M}$  estimates are  $< 0.9$  for binaries in ‘far-resonance’ configurations. The rather high  $\mathcal{M}$  estimates point to the possibility that a computationally cheaper resonant inspiral template bank may provide the desirable fitting factor ( $FF$ )  $\gtrsim 0.97$  for binaries influenced by spin-orbit resonances. This is because  $FF$ s are obtained by maximizing the  $\mathcal{M}$  over all the templates present in a certain bank of inspiral waveforms.

The paper is organized in the following way. In the next section, we briefly describe the spin-orbit resonances, detailed in [17] and the way to analyze the spin-orbit resonances in the inertial frame associated with  $\mathbf{j}_0$ . Various implications of our approach are probed in section 2.2. Our prescription to compute time-domain GW polarization states for inspiraling binaries experiencing the spin-orbit resonances is presented in section 3 along with certain preliminary data analysis implications. Conclusions are presented in section 4.

## 2. PN-accurate Equilibrium Configurations and their GW emission induced evolution

We first summarize [17] that probed the evolution of comparable mass precessing compact binaries initially residing in and around certain equilibrium spin configurations while invoking an orbital triad associated with  $\mathbf{L}_N$ . Section 2.2 contains our approach to describe the evolution of such binaries in an inertial frame based on  $\mathbf{j}_0$  along with various inferences.

### 2.1. Spin-orbit resonances in an orbital triad

Schnittman invoked an orbital triad based on  $\mathbf{L}_N$  to describe the dynamics of comparable mass spinning compact binary configurations as evident from figure 1 in [17]. In what follows, we use an orbital triad based on  $\mathbf{L}$  rather than  $\mathbf{L}_N$  to describe these binaries. For generic spinning compact binaries, the two spins are freely specified at the initial epoch by four angles, namely  $(\tilde{\theta}_1, \tilde{\phi}_1)$  and  $(\tilde{\theta}_2, \tilde{\phi}_2)$ . Therefore, the unit

vectors along the two spins read

$$\mathbf{s}_1(x_i) = \sin \tilde{\theta}_1 \cos \tilde{\phi}_1 \mathbf{a} + \sin \tilde{\theta}_1 \sin \tilde{\phi}_1 \mathbf{b} + \cos \tilde{\theta}_1 \mathbf{k}, \quad (1a)$$

$$\mathbf{s}_2(x_i) = \sin \tilde{\theta}_2 \cos \tilde{\phi}_2 \mathbf{a} + \sin \tilde{\theta}_2 \sin \tilde{\phi}_2 \mathbf{b} + \cos \tilde{\theta}_2 \mathbf{k}, \quad (1b)$$

where  $\mathbf{a}$  and  $\mathbf{b}$  may be identified with unit vectors  $\mathbf{e}_x$  and  $\mathbf{e}_y$  of [17]. Additionally, Schnittman equated  $\tilde{\phi}_1$  at the initial epoch to zero by noting that the orbital dynamics should be preserved under a rotation around  $\mathbf{k}$ . This implies that the orientations of these binaries, characterized by certain  $m, \eta, \chi_1, \chi_2$  and  $x$  (or  $\omega$ ) values, are specified by just *three* angular variables. These variables are  $(\tilde{\theta}_1, \tilde{\theta}_2, \Delta\tilde{\phi} = \tilde{\phi}_2 - \tilde{\phi}_1)$  where  $\Delta\tilde{\phi}$  specifies the relative angular separation of the two spins in the orbital plane while  $\tilde{\theta}_1$  and  $\tilde{\theta}_2$  define the orientations of  $\mathbf{s}_1$  and  $\mathbf{s}_2$  from  $\mathbf{k}$ , respectively. It is important to note that these angular variables vary over precessional and reactive time scales. Further, it may be recalled that the dynamical evolutions of such binaries involve three time-scales associated with the orbital, precessional and inspiral aspects of their dynamics and we denote these timescales by  $\tau_{\text{orb}}, \tau_{\text{pre}}$  and  $\tau_{\text{rr}}$ , respectively. It is not very difficult to infer that  $\tau_{\text{orb}} \ll \tau_{\text{pre}} \ll \tau_{\text{rr}}$  as they are associated with the Newtonian, 1PN and 2.5PN order terms in the PN-accurate orbital dynamics.

The equilibrium spin configurations, detailed in [17], are obtained by demanding that the first and second derivatives of  $\mathbf{s}_1 \cdot \mathbf{s}_2$  should be zero. Invoking the precessional equations for  $\mathbf{s}_1$  and  $\mathbf{s}_2$ , given by equations (7) below, it is easy to show that the above requirements are identical to equating  $\gamma$  and its time derivative to zero [17]. The expression for  $\gamma$  in the orbital triad reads

$$\gamma = \sin \tilde{\theta}_1 \sin \tilde{\theta}_2 \sin \Delta\tilde{\phi}, \quad (2)$$

and the requirement that  $\gamma = 0$  implies that  $\Delta\tilde{\phi}$  can take only one of the following two values:  $0^\circ$  or  $\pm 180^\circ$ . The constraints, namely  $\gamma = \dot{\gamma} = 0$ , allow us to numerically obtain  $\tilde{\theta}_2$  in terms of  $\tilde{\theta}_1$  for a binary characterized by specific values of  $\Delta\tilde{\phi}, m, \eta, \chi_1$  and  $\chi_2$ . In other words, the solutions to the above two constraints trace out one-dimensional curves in  $(\tilde{\theta}_1, \tilde{\theta}_2)$  space [17]. These solutions, having  $\Delta\tilde{\phi} = 0^\circ$  or  $\pm 180^\circ$ , stand for specific configurations where  $\mathbf{k}, \mathbf{s}_1$  and  $\mathbf{s}_2$  lie in a plane such that  $\mathbf{L}, \mathbf{s}_1$  and  $\mathbf{s}_2$  precess around  $\mathbf{J}$  with a roughly constant angular frequency on a precessional time scale. This prompted, as noted earlier, Schnittman to term these equilibrium configurations as certain spin-orbit resonant configurations. The requirement that  $\dot{\gamma} = 0$  may be written as an algebraic constraint invoking the precessional equations for  $\mathbf{k}, \mathbf{s}_1$  and  $\mathbf{s}_2$ . The constraint reads

$$(\boldsymbol{\Omega}_1 \times \mathbf{S}_1) \cdot [\mathbf{S}_2 \times (\mathbf{L} + \mathbf{S}_1)] = (\boldsymbol{\Omega}_2 \times \mathbf{S}_2) \cdot [\mathbf{S}_1 \times (\mathbf{L} + \mathbf{S}_2)], \quad (3)$$

where  $\boldsymbol{\Omega}_1$  and  $\boldsymbol{\Omega}_2$  provide precessional frequencies of  $\mathbf{s}_1$  and  $\mathbf{s}_2$ . Schnittman incorporated the contributions arising from the leading order spin-orbit and spin-spin interactions in to the above precessional frequencies and these contributions may be extracted from [8, 9].

To probe the effect of gravitational radiation reaction on these equilibrium spin configurations, Schnittman wrote down PN-accurate differential equations for the following four variables:  $z_1 = \mathbf{k} \cdot \mathbf{s}_1$ ,  $z_2 = \mathbf{k} \cdot \mathbf{s}_2$ ,  $\beta = \mathbf{s}_1 \cdot \mathbf{s}_2$  and  $\gamma = \mathbf{k} \cdot (\mathbf{s}_1 \times \mathbf{s}_2)$ . It is straightforward to figure out that these differential equations arise from the PN-accurate precessional equations for  $\mathbf{k}, \mathbf{s}_1$  and  $\mathbf{s}_2$  and therefore contain  $x$ . This implies that the differential equation for  $x$  that allows orbital frequency to slowly vary over  $\tau_{\text{rr}}$

may be invoked to incorporate the effects of gravitational radiation reaction on these variables. Therefore, the differential equations required to describe the dynamics of precessing compact binaries spiraling in from  $x = 10^{-3}$  in an orbital triad read

$$\dot{z}_1 = \frac{c^3}{Gm} x^3 \gamma \chi_2 \left\{ \frac{\delta_2}{q} - \frac{X_2^2}{2} - \frac{3}{2} x^{1/2} \eta \chi_1 z_1 \right\}, \quad (4a)$$

$$\dot{z}_2 = \frac{c^3}{Gm} x^3 \gamma \chi_1 \left\{ -\delta_2 q + \frac{X_1^2}{2} + \frac{3}{2} x^{1/2} \eta \chi_2 z_2 \right\}, \quad (4b)$$

$$\dot{\beta} = \frac{3}{2} \frac{c^3}{Gm} x^{5/2} \gamma \left\{ X_2 - X_1 + x^{1/2} (X_1^2 \chi_1 z_1 - X_2^2 \chi_2 z_2) \right\}, \quad (4c)$$

$$\begin{aligned} \dot{\gamma} = \frac{c^3}{Gm} x^{5/2} \left\{ \frac{3}{2} \frac{\delta m}{m} (\beta - z_1 z_2) + x^{1/2} \left[ \delta_1 q \chi_1 (z_2 - \beta z_1) \right. \right. \\ \left. \left. + \frac{\delta_2}{q} \chi_2 (\beta z_2 - z_1) + \frac{1}{2} X_1^2 \chi_1 (-z_2 - 2\beta z_1 + 3z_1^2 z_2) \right. \right. \\ \left. \left. + \frac{1}{2} X_2^2 \chi_2 (z_1 + 2\beta z_2 - 3z_1 z_2^2) \right] + \frac{3}{2} x \eta \chi_1 \chi_2 (z_1^2 - z_2^2) \right\}, \quad (4d) \end{aligned}$$

$$\dot{x} = \frac{64}{5} \frac{c^3}{Gm} \eta x^5, \quad (4e)$$

where  $z_1, z_2$  and  $\beta$  are specified by the angles  $\tilde{\theta}_1, \tilde{\theta}_2$  and  $\theta_{12}$ , respectively and we have verified that these equations are comparable to equations (A10) in [17]. In the above equations,  $q, \delta m, X_1$  and  $X_2$  stand for  $m_1/m_2, (m_1 - m_2), m_1/m$  and  $m_2/m$ , respectively while  $\delta_{1,2} = \eta/2 + 3(1 \mp \sqrt{1 - 4\eta})/4$ . The presence of  $x$  in the above expression indicates that these spin-orbit resonances can sweep through a substantial portion of the  $(\tilde{\theta}_1, \tilde{\theta}_2)$  space during the GW emission induced inspiral. The fact that  $\Delta\tilde{\phi}$  of a generic spinning compact binary can vary over the precessional timescale  $\tau_{\text{pre}}$  implies that the binary may approach the resonant values,  $\Delta\tilde{\phi} = 0^\circ$  or  $\pm 180^\circ$ , at some point during its lengthy PN-accurate inspiral regime, characterized by  $\tau_{\text{rr}}$ . It was argued that the orbital evolution of such generic spinning compact binaries will be heavily influenced by these spin-orbit resonances [17]. In practice, it is convenient to numerically solve the following *four* differential equations, namely  $dz_1/dx = \dot{z}_1/\dot{x}, dz_2/dx = \dot{z}_2/\dot{x}, d\beta/dx = \dot{\beta}/\dot{x}$  and  $d\gamma/dx = \dot{\gamma}/\dot{x}$  to probe how these binary configurations evolve under the combined influences of precessional and reactive dynamics from  $x = 10^{-3}$  to the late stages of inspiral prior to their coalescence.

Numerical integration of the above equations allowed [17] to infer that the initial equilibrium configurations, defined by  $\gamma = \dot{\gamma} = 0$  at  $x = x_i \equiv 10^{-3}$ , remain in their resonant plane during the inspiral regime. Moreover, gravitational radiation reaction forces binary spins, initially not in the resonant plane, to get locked and then librate about the equilibrium configurations during its inspiral from  $x_i$  to  $x_f$  ( $x = 0.1$ ). This was demonstrated by showing that the instantaneous phase difference  $\Delta\tilde{\phi}$  oscillates around  $0^\circ$  with steadily decreasing amplitude as evident from figure 5 in [17]. This spin alignment prompted Kesden *et al.* [18] to re-analyze these spin-orbit resonances in great detail and explore its implications for merging spinning BH binaries. Very recently, it was pointed out that the BH spins in comparable mass stellar mass BH binaries would preferentially lie in a resonant plane, characterized by  $\Delta\tilde{\phi} = 0^\circ$  or  $\Delta\tilde{\phi} = \pm 180^\circ$ , when GWs from such binaries enter the aLIGO frequency window [19]. The above conclusion requires an admissible assumption that the spins of the BH progenitors should be partially aligned with the orbital angular momentum due to

efficient tidal interactions. The ability of such binaries to stay essentially in a resonant plane is due to the combined effects of spin-orbit resonances and GW emission induced inspiral [19]. The authors also stated that it will be desirable to construct templates for inspiraling binaries influenced by the spin-orbit resonances.

In the next subsection, we evolve comparable mass binaries having spin configurations at  $x = 10^{-3}$  that are influenced by Schnittman's one parameter family of equilibrium solutions. We invoke an inertial frame associated with  $\mathbf{j}_0$  to specify both the orbital and spin angular momenta of such binaries and to describe their PN-accurate evolution. This is partly influenced by the observation that temporally evolving  $h_{\times,+}(t)$ , associated with spinning compact binaries, are usually computed in such an inertial frame. Therefore, the various inputs that are required to describe the spin-orbit resonances in the  $\mathbf{j}_0$  frame may be invoked while constructing inspiral templates associated with such binaries.

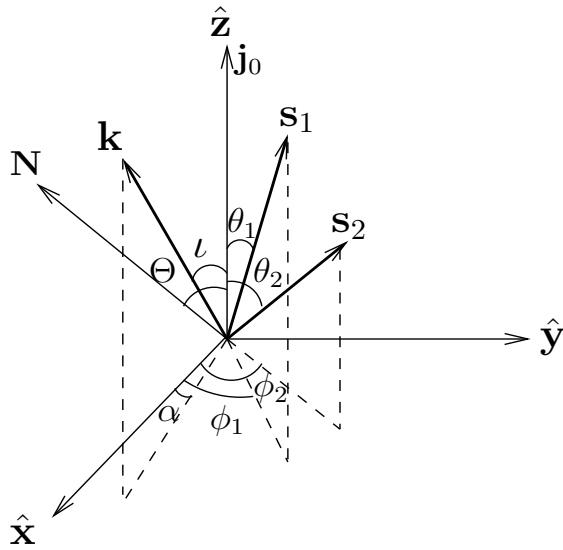


**Figure 1.** The inertial frame based on  $\mathbf{j}_0$ , the unit vector along the total angular momentum at the initial epoch. We let  $\mathbf{j}_0$  to point along the  $z$ -axis while the line of sight vector  $\mathbf{N}$  is defined by the constant angle  $\Theta$ . The angles that specify the unit vectors along the orbital and spin angular momenta, denoted by  $\mathbf{k}$ ,  $\mathbf{s}_1$  and  $\mathbf{s}_2$ , are displayed. We depict the projections of these unit vectors onto the  $x - y$  plane by dashed lines.

## 2.2. Spin-orbit resonances in an inertial frame defined by $\mathbf{j}_0$

We begin by describing how we specify the generic comparable mass spinning compact binaries, characterized by specific values of  $m, \eta, \chi_1$  and  $\chi_2$ , in an inertial frame associated with  $\mathbf{j}_0$  at large orbital separations ( $r \sim 500R_s$  or  $x = 10^{-3}$ ). We invoke the Cartesian coordinate system associated with this inertial frame such that the unit



vectors along  $\mathbf{S}_1$ ,  $\mathbf{S}_2$  and  $\mathbf{L}$  have the following  $(\hat{x}, \hat{y}, \hat{z})$  components:

$$\mathbf{s}_1 = (\sin \theta_1 \cos \phi_1, \sin \theta_1 \sin \phi_1, \cos \theta_1), \quad (5a)$$

$$\mathbf{s}_2 = (\sin \theta_2 \cos \phi_2, \sin \theta_2 \sin \phi_2, \cos \theta_2), \quad (5b)$$

$$\mathbf{k} = (\sin \iota \cos \alpha, \sin \iota \sin \alpha, \cos \iota). \quad (5c)$$

Therefore, it appears that we will require six angles, namely  $\theta_1$ ,  $\phi_1$ ,  $\theta_2$ ,  $\phi_2$ ,  $\iota$  and  $\alpha$ , to specify the orientation of our binary in the invariant frame as displayed in figure 1. However, the fact that the invariant frame is defined such that the total angular momentum at the initial epoch points along the  $z$ -axis allows us to estimate the initial  $x$  and  $y$  components of  $\mathbf{k}$  in terms of  $m$ ,  $\eta$ ,  $\chi_1$ ,  $\chi_2$ ,  $x_i$  and the values of  $\theta_1$ ,  $\phi_1$ ,  $\theta_2$  and  $\phi_2$  at the initial epoch. In other words, the initial  $x$  and  $y$  components of  $\mathbf{k}$  become dependent variables as we equate the  $x$  and  $y$  components of  $\mathbf{j}_0$  to zero. The resulting expression for the initial  $k_x$  and  $k_y$  read

$$k_x(x_i) = \sin \iota \cos \alpha = -\frac{Gm^2}{cL_i} \{X_1^2 \chi_1 \sin \theta_1 \cos \phi_1 + X_2^2 \chi_2 \sin \theta_2 \cos \phi_2\}, \quad (6a)$$

$$k_y(x_i) = \sin \iota \sin \alpha = -\frac{Gm^2}{cL_i} \{X_1^2 \chi_1 \sin \theta_1 \sin \phi_1 + X_2^2 \chi_2 \sin \theta_2 \sin \phi_2\}, \quad (6b)$$

where we employ the Newtonian accurate expression for  $|\mathbf{L}|$  at  $x_i$ , given by  $L_i = Gm^2 \eta / (c\sqrt{x_i})$ . Additionally, the initial value of  $k_z$  is uniquely given by  $k_z = +\sqrt{1 - k_x^2 - k_y^2}$  as  $\mathbf{L}$  almost point along  $\mathbf{J}$  at  $x_i$ . Therefore, the initial orientation of the orbital angular momentum are uniquely given by equations (6). This implies that the dynamics of such binaries are uniquely obtained by freely specifying the initial values of the four angular variables that provide the orientations of the two spins in the invariant frame.

We invoke the following set of three vectorial and one scalar differential equations to describe the inspiral dynamics of precessing spinning compact binaries, extracted from [8, 22, 23]. We first list the precessional equations for  $\mathbf{s}_1$  and  $\mathbf{s}_2$ , given by

$$\dot{\mathbf{s}}_1 = \frac{c^3}{Gm} x^{5/2} \left\{ \delta_1 (\mathbf{k} \times \mathbf{s}_1) + \frac{1}{2} x^{1/2} \left[ X_2^2 \chi_2 (\mathbf{s}_2 \times \mathbf{s}_1) - 3 X_2^2 \chi_2 (\mathbf{k} \cdot \mathbf{s}_2) (\mathbf{k} \times \mathbf{s}_1) - 3 \eta \chi_1 (\mathbf{k} \cdot \mathbf{s}_1) (\mathbf{k} \times \mathbf{s}_1) \right] \right\}, \quad (7a)$$

$$\dot{\mathbf{s}}_2 = \frac{c^3}{Gm} x^{5/2} \left\{ \delta_2 (\mathbf{k} \times \mathbf{s}_2) + \frac{1}{2} x^{1/2} \left[ X_1^2 \chi_1 (\mathbf{s}_1 \times \mathbf{s}_2) - 3 X_1^2 \chi_1 (\mathbf{k} \cdot \mathbf{s}_1) (\mathbf{k} \times \mathbf{s}_2) - 3 \eta \chi_2 (\mathbf{k} \cdot \mathbf{s}_2) (\mathbf{k} \times \mathbf{s}_2) \right] \right\}, \quad (7b)$$

where the terms proportional to  $x^{5/2}$  and  $x^3$  incorporate the dominant order spin-orbit and spin-spin interactions, respectively, for binaries moving in circular orbits. The  $x^3$  terms that are proportional to  $\eta$  are due to the quadrupole-monopole self interaction [23]. These terms were not included in the original analysis of Schnittman while they are present in the detailed analysis of [18]. The precessional motion of  $\mathbf{L}$  is described

by

$$\begin{aligned} \dot{\mathbf{k}} = \frac{c^3}{Gm} x^3 & \left\{ \delta_1 q \chi_1 (\mathbf{s}_1 \times \mathbf{k}) + \frac{\delta_2}{q} \chi_2 (\mathbf{s}_2 \times \mathbf{k}) \right. \\ & - \frac{3}{2} x^{1/2} \left[ \eta \chi_1 \chi_2 (\mathbf{k} \cdot \mathbf{s}_1) (\mathbf{s}_2 \times \mathbf{k}) + \eta \chi_1 \chi_2 (\mathbf{k} \cdot \mathbf{s}_2) (\mathbf{s}_1 \times \mathbf{k}) \right. \\ & \left. \left. + X_1^2 \chi_1^2 (\mathbf{k} \cdot \mathbf{s}_1) (\mathbf{s}_1 \times \mathbf{k}) + X_2^2 \chi_2^2 (\mathbf{k} \cdot \mathbf{s}_2) (\mathbf{s}_2 \times \mathbf{k}) \right] \right\}, \end{aligned} \quad (8)$$

and this equation arises from the conservation of total angular momentum which leads to  $\dot{\mathbf{L}} = -S_1 \dot{\mathbf{s}}_1 - S_2 \dot{\mathbf{s}}_2$ . We incorporated the effects of gravitational radiation reaction which causes the binaries to inspiral from  $x_i$  via

$$\frac{dx}{dt} = \frac{64}{5} \frac{c^3}{Gm} \eta x^5. \quad (9)$$

This equation requires the quadrupolar order GW luminosity along with the energy balance argument [22, 24]. We have verified that our inferences about the values of various angular variables at  $x_0$  are rather insensitive to the inclusion of PN corrections to the above expression for  $\dot{x}$ .

To describe PN-accurate evolution of comparable mass spinning compact binaries, we employ the Cartesian components of the precessional equations while numerically integrating equations (7), (8) and (9). In practice, we numerically solve the nine Cartesian components of the following three equations, namely  $d\mathbf{k}/dx$ ,  $d\mathbf{s}_1/dx$  and  $d\mathbf{s}_2/dx$  where, for example,  $d\mathbf{k}/dx = (d\mathbf{k}/dt)/\dot{x}$ . This is how we follow the orientations of the two spins and the orbital angular momenta from  $\mathbf{j}_0$  as these binaries inspiral from  $x_i$  to  $x_f$ . During our numerical integrations, the values of  $\theta_1, \phi_1, \theta_2, \phi_2, \iota$  and  $\alpha$  are extracted at the stipulated  $x$  values from the three Cartesian components of  $\mathbf{s}_1, \mathbf{s}_2$  and  $\mathbf{k}$  (we invoke equations (6) only once to estimate the initial Cartesian components of  $\mathbf{k}$ ). For example, the angular variables of the dominant spin, namely  $\theta_1$  and  $\phi_1$ , are obtained via  $\theta_1 = \cos^{-1}(s_{1z})$  and  $\phi_1 = \tan^{-1}(s_{1y}/s_{1x})$ . Similar expressions are employed to obtain  $\theta_2$  and  $\phi_2$  values while the orbital inclination  $\iota$  and  $\alpha$  values are also uniquely extracted from the three Cartesian components of  $\mathbf{k}$ . We are now in a position to explore PN evolution of binaries having spin configurations, at  $x = 10^{-3}$ , that are influenced by Schnittman's one parameter family of equilibrium solutions.

We begin by listing the expression for  $\gamma$  in terms of angular variables defined in the inertial frame:

$$\begin{aligned} \gamma = \sin \theta_1 \cos \theta_2 \sin \iota \sin(\phi_1 - \alpha) - \sin \theta_2 \cos \theta_1 \sin \iota \sin(\phi_2 - \alpha) \\ - \sin \theta_1 \sin \theta_2 \cos \iota \sin(\phi_1 - \phi_2). \end{aligned} \quad (10)$$

The fact that the equilibrium configurations are characterized by  $\gamma = 0$  implies  $\sin(\phi_1 - \phi_2) = \sin(\phi_1 - \alpha) = \sin(\phi_2 - \alpha) = 0$  for such configurations. Therefore, these special configurations are also characterized by  $\Delta\phi = \phi_2 - \phi_1 = 0^\circ$  or  $\pm 180^\circ$  in our inertial frame. Note that  $\gamma = 0$  forces certain restriction on the initial  $\alpha$  value and it turned out to be consistent with initial  $\alpha$  value via equations (6). For numerically obtaining Schnittman equilibrium configurations in the inertial frame, we employ the following expression for  $\gamma$  involving the Cartesian components of  $\mathbf{k}$

$$\begin{aligned} \gamma = k_x(\sin \theta_1 \sin \phi_1 \cos \theta_2 - \sin \theta_2 \sin \phi_2 \cos \theta_1) + k_y(\sin \theta_2 \cos \phi_2 \cos \theta_1 \\ - \sin \theta_1 \cos \phi_1 \cos \theta_2) + k_z \sin \theta_1 \sin \theta_2 \sin(\phi_2 - \phi_1), \end{aligned} \quad (11)$$

where we express  $k_x$ ,  $k_y$  and  $k_z$  in terms of the Cartesian components of  $\mathbf{s}_1$  and  $\mathbf{s}_2$  invoking equations (6). The associated expression for  $\dot{\gamma}$  is given by

$$\begin{aligned} \dot{\gamma} = \frac{c^3}{Gm} x^{5/2} & \left\{ \frac{3}{2} \frac{\delta m}{m} (\beta - z_1 z_2) + x^{1/2} \left[ \delta_1 q \chi_1 (z_2 - \beta z_1) \right. \right. \\ & + \frac{\delta_2}{q} \chi_2 (\beta z_2 - z_1) + \frac{1}{2} X_1^2 \chi_1 (-z_2 - 2\beta z_1 + 3z_1^2 z_2) \\ & + \frac{1}{2} X_2^2 \chi_2 (z_1 + 2\beta z_2 - 3z_1 z_2^2) + \frac{3}{2} \eta (\beta - z_1 z_2) (\chi_1 z_1 - \chi_2 z_2) \left. \right] \\ & + \frac{3}{2} x \left[ \eta \chi_1 \chi_2 (z_1^2 - z_2^2) + X_1^2 \chi_1^2 z_1 (z_1 \beta - z_2) \right. \\ & \left. \left. + X_2^2 \chi_2^2 z_2 (z_1 - \beta z_2) \right] \right\}, \end{aligned} \quad (12)$$

where,  $z_1$ ,  $z_2$  and  $\beta$  are functions of  $\theta_1$ ,  $\phi_1$ ,  $\theta_2$ ,  $\phi_2$ . These three dot products in the invariant frame may be written as

$$z_1 = \mathbf{k} \cdot \mathbf{s}_1 = k_x \sin \theta_1 \cos \phi_1 + k_y \sin \theta_1 \sin \phi_1 + k_z \cos \theta_1 \quad (13a)$$

$$z_2 = \mathbf{k} \cdot \mathbf{s}_2 = k_x \sin \theta_2 \cos \phi_2 + k_y \sin \theta_2 \sin \phi_2 + k_z \cos \theta_2 \quad (13b)$$

$$\beta = \mathbf{s}_1 \cdot \mathbf{s}_2 = \sin \theta_1 \sin \theta_2 \cos(\phi_1 - \phi_2) + \cos \theta_1 \cos \theta_2. \quad (13c)$$

It should be noted that the above expression for  $\dot{\gamma}$  is not identical to equation (4d) and this is due to the use of fully 2PN-accurate precessional equations that include the quadrupole-monopole self interaction terms in this subsection [23]. Let us note that we need to express  $k_x$ ,  $k_y$  and  $k_z$ , appearing in the above expressions for  $z_1$  and  $z_2$ , in terms of the Cartesian components of  $\mathbf{s}_1$  and  $\mathbf{s}_2$  with the help of equations (6) while dealing with the above equation for  $\dot{\gamma}$ . We obtain Schnittman's equilibrium configurations by simultaneously equating equations (11) and (12) for  $\gamma$  and  $\dot{\gamma}$  to zero. This allows us to numerically obtain  $\theta_2$  values in terms of  $(\theta_1, \phi_1)$  for two specific values of  $\Delta\phi$ , namely  $\Delta\phi = 0^\circ$  or  $\pm 180^\circ$  and define the equilibrium configurations in the invariant frame. These configurations are such that initial  $\alpha$  value, obtained via equations (6), is consistent with the requirement arising from equating  $\gamma$ , given by equation (10), to zero. Additionally, the extracted values of the angular variables are also consistent with the requirement that the initial  $x$  and  $y$  components of  $\mathbf{J}$  should be zero. It should be noted that in our approach Schnittman's equilibrium configurations are specified by three angular variables, namely  $(\theta_1, \phi_1, \Delta\phi)$ , compared to two in [17]. This is merely a consequence of invoking the Cartesian components to obtain these special configurations and we have verified that our results do not depend on the initial value of  $\phi_1$ . In what follows, we consider maximally spinning BH binaries with  $m = 20M_\odot$  and  $q = 11/9$  while choosing the initial  $\phi_1$  to be  $45^\circ$ . We are now in a position to explore and evolve binaries having spin configurations that are influenced by Schnittman's one parameter family of equilibrium solutions.

We begin by displaying Schnittman's equilibrium configurations in our inertial frame for maximally spinning BH binaries with  $q = 11/9$  as one dimensional curves in the  $(\theta_1, \theta_2)$  plane (see figure 2). These curves, influenced by figures 2 and 3 in [17], are for binaries residing at various orbital separations starting from  $r \sim 500 R_g$ . The equilibrium solutions having  $\Delta\phi = 0^\circ$  are displayed in the left panel and the right panel plots are for  $\Delta\phi = 180^\circ$  equilibrium configurations. These plots are fairly similar to the  $\mathbf{k} \cdot \mathbf{s}_1 - \mathbf{k} \cdot \mathbf{s}_2$  plots in figure 1 of [18] that depict Schnittman's equilibrium

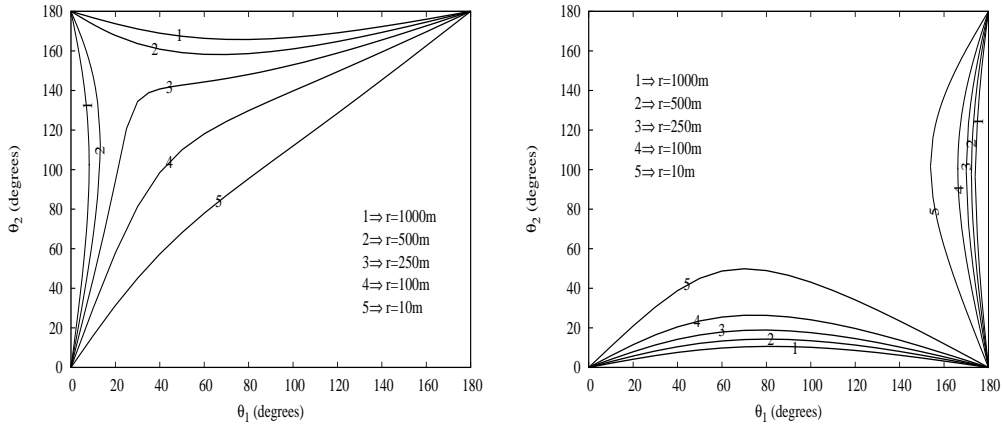


**Figure 2.** Schnittman’s equilibrium solutions in the  $\hat{j}_0$ -based inertial frame. These curves are obtained by equating the equations (11) and (12) to zero for maximally spinning BH binaries with  $q = 11/9$ . The resonant configurations with  $\Delta\phi = 0^\circ$  are displayed on the left panel while the right panel plots are for the  $\Delta\phi = 180^\circ$  equilibrium configurations.

configurations in an orbital triad. We observe that  $\Delta\phi = 0^\circ$  resonances have  $\theta_2 > \theta_1$  and therefore the associated plots appear above the  $\theta_2 = \theta_1$  diagonal while the reverse holds good for the  $\Delta\phi = 180^\circ$  equilibrium configurations. For binaries having  $\theta_1 < 10^\circ$  at large orbital separations like  $r \sim 500 R_s$ , the  $\Delta\phi = 0^\circ$  equilibrium solutions lie along two curves. This allows many more spin configurations to lie in the close neighborhood of such resonant configurations. Similar statement apply for binaries having  $\theta_1(x_i) > 160^\circ$  while dealing with  $\Delta\phi = 180^\circ$  equilibrium configurations. We also observe that as these binaries inspiral from  $x = 10^{-3}$ , the  $\Delta\phi = 0^\circ$  equilibrium solutions sweep through a larger area of the  $(\theta_1, \theta_2)$  plane compared to the  $\Delta\phi = 180^\circ$  configurations. All these conclusions are consistent with the studies that invoked  $L_N$ -based non-inertial orbital triad to describe these equilibrium solutions [17, 18].

We move on to probe the effect of GW induced damping on these equilibrium configurations. The plots of figure 3 probe the evolution of three  $\Delta\phi = 0^\circ$  equilibrium solutions while terminating the inspiral at  $x_0$ . These configurations are characterized by three values of  $\theta_1(x_i)$ , namely  $10^\circ$ ,  $20^\circ$  and  $30^\circ$ . The  $\theta_1(x_i)$  values are influenced by the inference that the traditional formation scenarios for comparable mass BH binaries likely to result in spin-orbit misalignments  $\leq 30^\circ$  [25]. Note that this investigation actually provided estimates for spin-orbit misalignments, namely  $\hat{\theta}_1$  values, at large orbital separations. The large orbital separations allowed us to let  $\hat{\theta}_1(x_i) \sim \theta_1(x_i)$ . Secular increments/decrements in the  $\theta_1(x)/\theta_2(x)$  values are clearly visible while  $\iota$  experiences secular increase during the inspiral. It turned out that the secular evolution of various angular variables is a characteristic of binaries lying in the resonant planes, specified by either  $\Delta\phi = 0^\circ$  or  $\Delta\phi = \pm 180^\circ$ . More importantly, we find that  $\theta_2 > \theta_1 > \iota$  at the initial frequencies of GW detectors and typical values of  $\iota(x_0)$  are  $> 10^\circ$ .

In figure 4, we explore how the above angular variables evolve for  $\theta_1(x_i)$  values lying below  $10^\circ$ . These configurations can arise in the formation scenarios involving

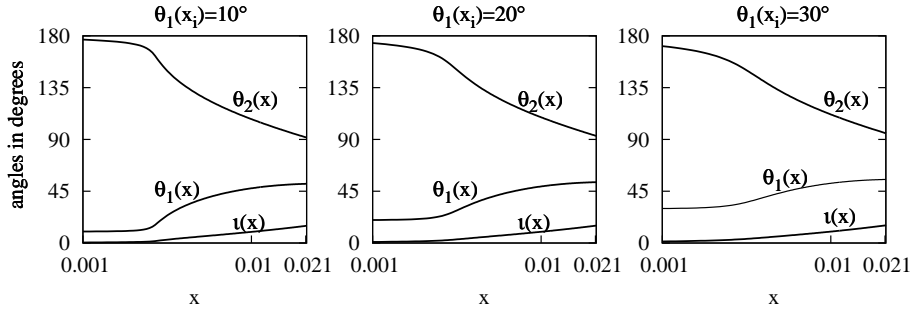


**Figure 3.** Semi-log plots that follow the GW induced evolution of the orientations of  $\mathbf{s}_1, \mathbf{s}_2$  and  $\mathbf{k}$  from  $\mathbf{j}_0$  for our typical BH binaries. We follow the evolution in the  $[x_i - x_0]$  interval for three spin configurations that satisfy Schnittman's  $\Delta\phi = 0^\circ$  equilibrium solutions at  $x_i$ . It should be evident that  $\theta_2 > \theta_1 > \iota$  at  $x_0$  and these angular variables evolve secularly in the  $x$  interval.

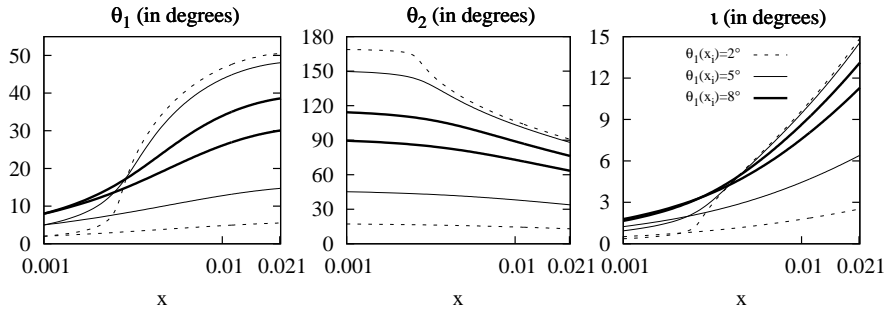


**Figure 4.** Plots for  $\theta_1(x), \theta_2(x)$  and  $\iota(x)$  associated with the  $\Delta\phi = 0^\circ$  equilibrium solutions for three  $\mathbf{s}_1$  orientations that are  $\leq 10^\circ$  at  $x_i$ . For a given  $\theta_1(x_i)$  value, these spin configurations can have multiple resonant  $\theta_2(x_i)$  values. This may be attributed to the presence of two equilibrium curves at  $r = 1000m$  in the  $(\theta_1, \theta_2)$  plane. We follow binaries having two distinct  $\theta_2(x_i)$  values for three configurations having  $\theta_1(x_i)$  values that are  $\leq 10^\circ$ . We observe that  $\theta'_2 > \theta'_1 > \iota'$  for all these binary configurations while small values of these angular variables indicate the influence of efficient tides during their formation.

rather efficient tides along with isotopic or polar supernovae kicks. This should be evident from the green dots in the  $a = 1000M$  scatter plots in figures 5 and 6 of [19]. For the plots in figure 4, we let  $\theta_1(x_i)$  to take the three values, namely  $2^\circ, 5^\circ$  and  $8^\circ$ . These  $\theta_1$  spin configurations can have multiple resonant  $\theta_2(x_i)$  values and this is due to the presence of two equilibrium curves at  $r = 1000m$  in the  $(\theta_1, \theta_2)$  plane. The evolution of  $\theta_1, \theta_2$  and  $\iota$  turned out to be quite different for resonant  $\theta_2(x_i)$  values lying below and above  $90^\circ$ . For example,  $\iota(x_0)$  and  $\theta_1(x_0)$  values are noticeably higher for binaries having their resonant  $\theta_2(x_i)$  values that are above  $90^\circ$ . We note that binaries with  $\iota' \leq 10^\circ$  can have formation scenarios involving either isotopic or polar kicks along with efficient tides. However, binaries with substantially higher  $\theta'_1$  and  $\theta'_2$  values demand a binary formation channel involving efficient tides and isotopic supernovae kicks. This is mainly because such a formation channel naturally allows the less massive spin to lie in the neighborhood of  $180^\circ$  from  $\mathbf{j}_0$  at large orbital separations (see figure 5 of [19]).

We also explored the PN-accurate evolution of binaries influenced by the  $\Delta\phi = 180^\circ$  equilibrium solutions and the results are displayed in figure 5. The chosen values of  $\theta_1(x_i)$  are  $30^\circ$ ,  $90^\circ$  and  $150^\circ$ . These initial  $\theta_1$  choices are clearly influenced by the SMR binary formation channel that also experience efficient tides and isotopic kicks [19] (see their  $a = 1000M$  red scatter plots in figure 5). These plots clearly show that  $\theta'_1 > \theta'_2 > \iota'$  and typical  $\iota(x_0)$  values are in the  $[2^\circ - 10^\circ]$  range. We also explored the inspiral dynamics of binaries having  $\theta_1(x_i)$  lying below  $30^\circ$  and the results are shown in figure 6. Interestingly, we find  $\iota'$  values are essentially negligible for initial  $\theta_1$  values below  $15^\circ$ . It should be noted that these  $\theta_1(x_i)$  and  $\theta_2(x_i)$  values are consistent with formation channels involving efficient tides while having both isotropic and polar supernovae kicks.

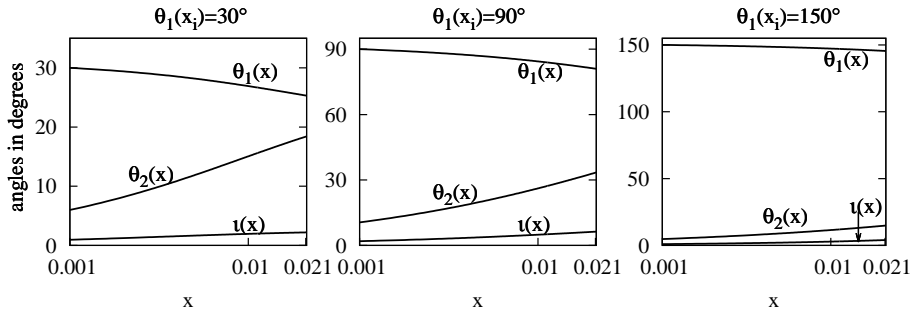


**Figure 5.** Plots for binaries that satisfy Schnittman’s  $\Delta\phi = 180^\circ$  equilibrium configurations at  $x_i$ . The figure follows reactive evolution of the angles that specify the orientations of  $\mathbf{s}_1$ ,  $\mathbf{s}_2$  and  $\mathbf{k}$  from  $\mathbf{j}_0$  for three spin configurations. The initial  $\theta_1(x_i)$  values are influenced by [19] and we terminate the evolution at  $x_0$ . We observe that  $\theta'_1 > \theta'_2 > \iota'$  while typical  $\iota(x_0)$  values are of the order of few degrees.

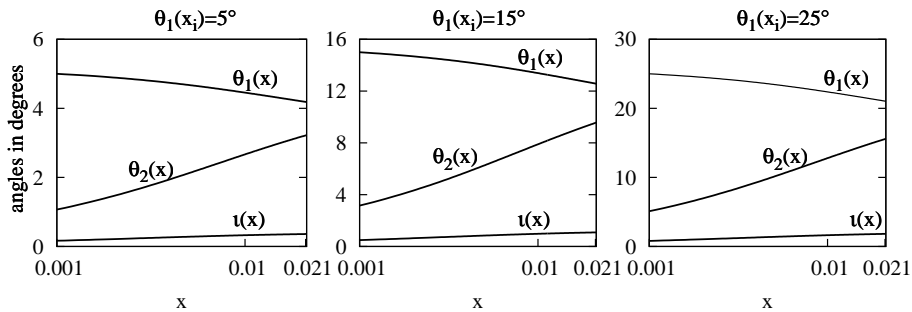


**Figure 6.** Plots, similar to figure 5, for maximally spinning BH binaries with  $q = 11/9$ . These spin configurations satisfy the  $\Delta\phi = 180^\circ$  equilibrium solutions at  $x_i$ . The three  $\theta_1(x_i)$  values are influenced by [19] and are associated with the SMR binary formation scenario involving efficient tides and polar kicks. The orbital angular momentum essentially get aligned with  $\mathbf{j}_0$  at  $x_0$  for these binaries.

A close inspection of the  $\theta_1(x)$ ,  $\theta_2(x)$  and  $\iota(x)$  plots of figures 3, 4, 5 and 6 reveals the following interesting point. We infer that GWs from inspiraling resonant binaries should allow us, in principle, to distinguish between the models of their

formation involving the SMR or RMR scenarios, detailed in [19]. This requires accurate measurements of  $\theta'_1, \theta'_2$  and  $\iota'$  values that provide the orientations of  $\mathbf{s}_1, \mathbf{s}_2$  and  $\mathbf{k}$  from  $\mathbf{j}_0$  when GWs enter interferometric frequency windows. We find that the SMR scenario binaries tend to have  $\theta'_1 > \theta'_2 > \iota'$ . The typical values of  $\iota'$  are expected to lie below  $10^\circ$ . However, negligible  $\iota'$  values are likely for binaries whose formation scenario involved very efficient tides. In contrast, in the RMR scenario binaries likely to have  $\theta'_2 > \theta'_1 > \iota'$  and typical  $\iota'$  values are  $> 10^\circ$ . Binaries with non-negligible  $\iota'$  values in the range of few degrees demand RMR formation scenario supplemented by efficient tides. The above deductions obviously require the crucial inference of [19] that the SMR and RMR formation channels lead to  $\Delta\phi = \pm 180^\circ$  and  $\Delta\phi = 0$  resonances, respectively. We also gather from our numerical integrations that  $\Delta\phi, \gamma$  and  $\dot{\gamma} \equiv (Gm/c^3 x^{5/2})\dot{\gamma}$  essentially remain constant in the  $[10^{-3}, 0.1] x$  interval for the above two families of equilibrium solutions. The negligible evolution of these quantities validate Schnittman's observation that the equilibrium configurations remain in their associated resonant plane during the inspiral. Note that the expression for  $\dot{\gamma}$  allows us to follow the variations in the angular part of  $\dot{\gamma}$ , given by equation (12).

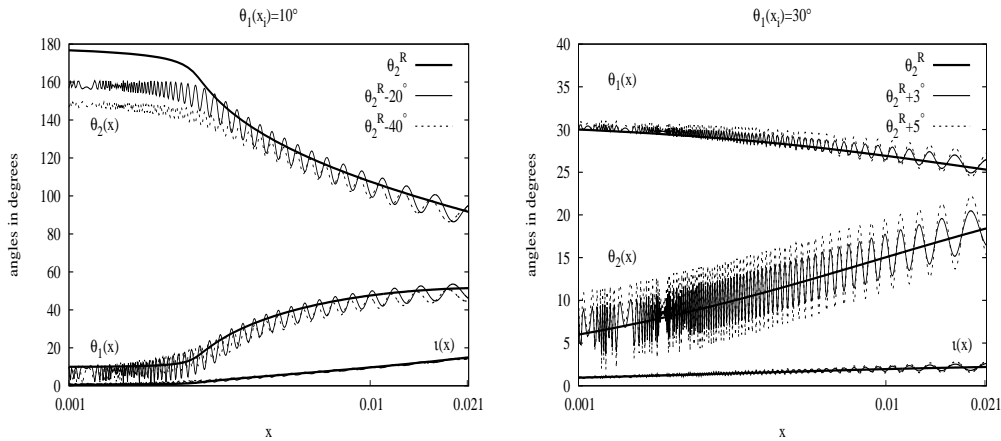


**Figure 7.** We depict the evolution of  $\theta_1, \theta_2$  and  $\iota$  for spin configurations that do not satisfy Schnittman's equilibrium solutions at  $x_i$ . These non-resonant configurations are constructed by allowing  $\theta_2(x_i)$  to be different from their actual resonant values. The left/right panel plots are for binaries influenced by the  $\Delta\phi = 0^\circ/180^\circ$  spin-orbit resonances. The constraints that distinguish binaries initially in the  $\Delta\phi = 0^\circ$  or  $\pm 180^\circ$  equilibrium solutions are also respected by these non-resonant spin configurations. During their GW induced inspiral, these configurations get 'captured' by the spin-orbit resonances and their angular variables librate about the equilibrium solutions.

It turns out that the above listed constraints also apply for binary configurations that do not satisfy Schnittman's equilibrium solutions at  $x_i$ . In figure 7, we present  $\theta_1(x), \theta_2(x)$  and  $\iota(x)$  plots for binaries that do not lie in the  $\Delta\phi = 0^\circ$  and  $\Delta\phi = 180^\circ$  resonant planes. This is implemented by choosing  $\theta_2(x_i)$  values that are noticeably different from their resonant values at  $x_i$ . The left panel plots clearly show that  $\theta'_2 > \theta'_1 > \iota'$  and we clearly notice the influence of the  $\Delta\phi = 0^\circ$  spin-orbit resonances. The values of plotted quantities at  $x_0$  in the right panel plots are consistent with the SMR formation scenario for these binaries. We again observe that  $\theta'_1 > \theta'_2 > \iota'$

as required for binaries influenced by the  $\Delta\phi = 180^\circ$  spin-orbit resonances. We have evolved a number of similar binary configurations and the resulting values of  $\theta_1, \theta_2$  and  $\iota$  at  $x_0$  indeed follow the constraints satisfied by binaries that lie in the  $\Delta\phi = 0^\circ$  and  $\Delta\phi = 180^\circ$  resonant planes at  $x_i$ . Therefore, we conclude that GWs from inspiraling spinning binaries that are influenced by the spin-orbit resonances should also allow us to distinguish between the models of their formation involving the SMR or RMR scenarios, detailed in [19]. In appendix, we follow the evolution of spin configurations that do not satisfy the equilibrium solution at  $x_i$ . This is to probe the behavior of various dynamical variables like  $\Delta\phi, \gamma, \dot{\gamma}$  and  $\cos^{-1}(\mathbf{s}_1 \cdot \mathbf{s}_2)$  as such binaries evolve to  $x_0$ .

We also explored the ability of GW measurements to distinguish freely precessing binaries from those influenced by the above two families of spin-orbit resonances. The freely precessing binaries are expected to have  $\theta_1(x_i) \sim \theta_2(x_i)$  as tidal interactions play no significant role during their formation [19]. Moreover, the  $\theta_1(x_i)$  and  $\theta_2(x_i)$  values can vary essentially between  $0^\circ$  and  $180^\circ$ . It turns out that these binaries are not affected by the spin-orbit resonances during their GW induced inspiral from  $x_i$  to  $x_0$ . With the help of our numerical integrations, we find that these binaries can mimic the constraints on the  $\theta'_1, \theta'_2$  and  $\iota'$  values that are satisfied by the two types of resonant binaries. However, the  $\theta_{12}(x_0)$  values for freely precessing binaries will not satisfy certain specific relations involving  $\theta_1(x_0)$  and  $\theta_2(x_0)$  values. This is important as binaries under the influence of  $\Delta\phi = 0^\circ$  ( $\Delta\phi = \pm 180^\circ$ ) spin-orbit resonances are expected to have  $\theta_{12}(x_0) \sim \theta'_2 - \theta'_1$  ( $\theta_{12}(x_0) \sim \theta'_1 + \theta'_2$ ) and these relations essentially arise from equation (13c). Therefore, this additional constraint may be invoked to separate the freely precessing binaries from the two families of resonant binaries. To illustrate these points, we provide following two examples. In the first case, we evolve our typical BH binary having  $\theta_1(x_i) = \theta_2(x_i) = 40^\circ$  to  $x_0$  and the resulting values of  $\theta_1, \theta_2, \iota$  and  $\theta_{12}$  at  $x_0$  are around  $30^\circ, 46^\circ, 5^\circ$  and  $66^\circ$ , respectively. The values of the first three angular variables indicate that the binary can be disguise as one under the influence of the  $\Delta\phi = 0^\circ$  spin-orbit resonance. However, the binary's  $\theta_{12}(x_0)$  value does not obey the required relation, namely  $\theta_{12}(x_0) \sim \theta'_2 - \theta'_1$  and this allows us to identify it as a freely precessing one. In the second example, we let  $\theta_1(x_i) = \theta_2(x_i) = 80^\circ$  and the resulting  $\theta'_1, \theta'_2, \iota'$  and  $\theta_{12}(x_0)$  values are around  $91^\circ, 36^\circ, 14^\circ$  and  $60^\circ$ , respectively. Therefore, it is possible to mistake the configuration as one influenced by the  $\Delta\phi = \pm 180^\circ$  spin-orbit resonances, if we restrict our attention to the values of  $\theta'_1, \theta'_2$  and  $\iota'$ . Fortunately, the fact that  $\theta_{12}(x_0) \neq \theta'_1 + \theta'_2$  allows us to correctly identify the binary configuration as a freely precessing one. These arguments indicate that the accurate measurements of  $\theta'_1, \theta'_2, \iota'$  and  $\theta_{12}(x_0)$  values are crucial to distinguish the three possible families of inspiraling comparable mass spinning binaries.

There exists a number of investigations that probed the accuracies with which GW observations can estimate various parameters of precessing compact binaries, relevant for both space and ground based GW observatories [26, 27, 28, 29]. These Fisher information matrix based studies indicate that precessing spins along with amplitude corrected GW polarization states tend to improve measurement accuracies of various intrinsic and extrinsic parameters that characterize the inspiral waveform. The intrinsic parameters include  $m, q, \chi_1, \chi_2$  and angular variables like  $\tilde{\theta}_1$  while extrinsic parameters refer to the initial phase and angles like  $\Theta$ . Very recently, [30] explored measurement accuracies for precessing BH-NS binaries with the help of Markov-chain Monte Carlo simulations. This detailed study observed that the mass parameters can be better constrained compared to their non-precessing counterparts. Additionally,



various binary orientation parameters can be measured with reasonable accuracies of the order of few percents for fairly loud GW inspiral signals having signal-to-noise-ratio  $\rho \simeq 20$ . It will be desirable to pursue a similar study while invoking our approach to compute  $h_{\times,+}(t)$  associated with spinning compact binaries influenced by spin-orbit resonances. Such an analysis would allow one to estimate the accuracies with which aLIGO observations can estimate the orientations of  $\mathbf{k}$ ,  $\mathbf{s}_1$  and  $\mathbf{s}_2$  from  $\mathbf{j}_0$ . This in turn should allow us to distinguish between the two possible families of spin-orbit resonances in a quantitative manner and to constrain possible binary formation scenarios.

In the next section, we provide a prescription to compute  $h_{\times,+}(t)$  associated with spinning binaries experiencing the spin-orbit resonances that inspiral through the frequency windows of GW detectors. We discuss implications of our approach that includes probing the consequence of such binaries not staying in a resonant plane when they enter the aLIGO frequency window. We also discuss certain preliminary data analysis implications of these templates.

### 3. GW phasing for compact binaries experiencing the spin-orbit resonances

We adapt an approach, detailed in [15], to accurately model temporally evolving GW polarization states for inspiraling compact binaries experiencing the spin-orbit resonances. In this approach, one invokes  $\mathbf{L}$  rather than its Newtonian counterpart to describe the binary orbits and the two spins are initially specified in a  $\mathbf{j}_0$ -based inertial frame. This should allow us to incorporate easily various inputs from the previous section into the present task. In what follows, we briefly describe the phasing approach of [15] and we begin by listing the following expressions for  $h_{\times}$  and  $h_{+}$ , computed using the Newtonian accurate expression for the quadrupole moment of the

binary. These expressions, derived in [15], read

$$\begin{aligned}
 h_{\times}|_{\text{Q}} = \frac{2G\mu v^2}{c^4 R'} & \left\{ (1 - \cos \iota) S_{\theta} \sin \iota \sin(\alpha - 2\Phi) \right. \\
 & - (1 + \cos \iota) S_{\theta} \sin \iota \sin(\alpha + 2\Phi) \\
 & - \frac{1}{2}(1 + 2 \cos \iota + \cos^2 \iota) C_{\theta} \sin(2\alpha + 2\Phi) \\
 & \left. - \frac{1}{2}(1 - 2 \cos \iota + \cos^2 \iota) C_{\theta} \sin(2\alpha - 2\Phi) \right\}, \quad (14a)
 \end{aligned}$$

$$\begin{aligned}
 h_{+}|_{\text{Q}} = \frac{2G\mu v^2}{c^4 R'} & \left\{ \left( \frac{3}{2} \cos^2 \iota - \frac{3}{2} \right) (1 - C_{\theta}^2) \cos 2\Phi \right. \\
 & - (1 + \cos \iota) S_{\theta} C_{\theta} \sin \iota \cos(2\Phi + \alpha) \\
 & - \frac{1}{4}(\cos^2 \iota + 2 \cos \iota + 1) (1 + C_{\theta}^2) \cos(2\alpha + 2\Phi) \\
 & - \frac{1}{4}(\cos^2 \iota - 2 \cos \iota + 1) (1 + C_{\theta}^2) \cos(2\alpha - 2\Phi) \\
 & - S_{\theta} C_{\theta} \sin \iota \cos \iota \cos(\alpha - 2\Phi) \\
 & \left. + S_{\theta} C_{\theta} \sin \iota \cos(\alpha - 2\Phi) \right\}, \quad (14b)
 \end{aligned}$$

where  $v^2/c^2$ ,  $C_{\theta}$  and  $S_{\theta}$  stand for  $(Gm\dot{\Phi}/c^3)^{2/3}$ ,  $\cos \Theta$  and  $\sin \Theta$ , respectively. It should be obvious that to obtain  $h_{\times,+}|_{\text{Q}}(t)$ , associated with precessing spinning compact binaries inspiraling along circular orbits, we need to specify how  $\iota$ ,  $\alpha$ ,  $\Phi$  and  $\dot{\Phi}$  are varying in time. This is achieved by simultaneously solving (numerically) the differential equations for the Cartesian components of the fully 2PN-accurate expressions for  $\mathbf{s}_1$ ,  $\mathbf{s}_2$  and  $\mathbf{k}$ , given by equations (7) and (8), in the  $\mathbf{j}_0$ -based inertial frame along with PN-accurate differential equations for  $\Phi$  and  $x$ . The differential equation for  $\Phi$  is given by

$$\dot{\Phi} = \frac{x^{3/2}}{(Gm/c^3)} - \cos \iota \dot{\alpha}, \quad (15)$$

where we invoked the definition  $\omega = v/r$  and employed the expression for  $\mathbf{v}$  in the co-moving triad to derive the above differential equation for  $\Phi$  [9, 15]. The effect of GW emission on the above precessional dynamics is incorporated by describing how  $x$  evolves in time. We use the following fully 2PN accurate expression for  $\dot{x}$  that includes 2PN-accurate non-spinning, 1.5PN order spin-orbit and 2PN order quadrupole-monopole and spin-spin self interactions [9, 31, 32, 33, 34]. The resulting

expression reads

$$\begin{aligned}
 \frac{dx}{dt} = & \frac{64}{5} \frac{c^3}{Gm} \eta x^5 \left\{ 1 + x \left[ -\frac{743}{336} - \frac{11\eta}{4} \right] + 4\pi x^{3/2} \right. \\
 & + \frac{x^{3/2}}{12} \left[ (-188 X_1 + 75\sqrt{1-4\eta}) X_1 \chi_1 (\mathbf{s}_1 \cdot \mathbf{k}) \right. \\
 & \left. + (-188 X_2 - 75\sqrt{1-4\eta}) X_2 \chi_2 (\mathbf{s}_2 \cdot \mathbf{k}) \right] \\
 & + x^2 \left[ \left( \frac{34103}{18144} + \frac{13661}{2016} \eta + \frac{59}{18} \eta^2 \right) \right. \\
 & - \frac{1}{48} \eta \chi_1 \chi_2 \left( 247 (\mathbf{s}_1 \cdot \mathbf{s}_2) - 721 (\mathbf{s}_1 \cdot \mathbf{k}) (\mathbf{s}_2 \cdot \mathbf{k}) \right) \\
 & + X_1^2 \chi_1^2 \left( \frac{5}{2} (3 (\mathbf{k} \cdot \mathbf{s}_1)^2 - 1) + \frac{1}{96} (7 - (\mathbf{k} \cdot \mathbf{s}_1)^2) \right) \\
 & \left. \left. + X_2^2 \chi_2^2 \left( \frac{5}{2} (3 (\mathbf{k} \cdot \mathbf{s}_2)^2 - 1) + \frac{1}{96} (7 - (\mathbf{k} \cdot \mathbf{s}_2)^2) \right) \right] \right\}. \quad (16)
 \end{aligned}$$

Therefore, we numerically solve eleven coupled differential equations to obtain  $h_{\times,+}|_{\mathcal{Q}}(t)$ . These equations include the nine equations for the Cartesian components of  $\mathbf{k}$ ,  $\hat{\mathbf{s}}_1$  and  $\hat{\mathbf{s}}_2$ , given by equations (7) and (8) in the  $\mathbf{j}_0$ -based inertial frame, displayed in figure 1 along with PN-accurate differential equations, namely equations (15) and (16) for  $\Phi$  and  $x$ . At every epoch, we extract the values of  $\alpha$ ,  $\iota$ ,  $\Phi$  and  $\dot{\Phi}$  and hence evaluate the expressions for  $h_{\times,+}|_{\mathcal{Q}}$ , given by equations (14). This is how we obtain temporally evolving GW polarization states for *regular* inspiraling precessing compact binaries. Let us note that we extract the angular variables  $\iota$  and  $\alpha$  from the three Cartesian components of  $\mathbf{k}$  at every epoch with the help of  $\iota = \cos^{-1}(k_z)$  and  $\alpha = \tan^{-1}(k_y/k_x)$ .

It should be obvious that we require to impose certain restrictions on the angles specifying the initial orientations of  $\mathbf{s}_1$ ,  $\mathbf{s}_2$  and  $\mathbf{k}$  at  $x_0$  to obtain  $h_{\times,+}|_{\mathcal{Q}}(t)$  associated with inspiraling spinning compact binaries that belong to Schnittman's equilibrium configurations. These restrictions are imposed in few steps and we begin by specifying  $(m_1, m_2, \chi_1, \chi_2)$  values making sure that  $m_1 \sim m_2$ . We also freely specify the values of  $(\theta_1, \phi_1)$  at  $x_0$  and these two angles provide the initial orientation of the more massive BH spin  $\mathbf{s}_1$  at the initial aLIGO frequency in our  $\mathbf{j}_0$ -based inertial frame. The requirement that  $\gamma$ , given by equation (10), should be zero allows us to let  $\phi_2 = \phi_1$  at  $x_0$  (in other words, we are focusing on the  $\Delta\phi = 0^\circ$  equilibrium configurations). These are the only inputs required to numerically obtain the  $\theta_2(x_0)$  value and this is achieved, as noted earlier, by equating the following expression for  $\dot{\gamma}$  to zero. The relevant expression for  $\dot{\gamma}$  reads

$$\begin{aligned}
 \dot{\gamma} = & \frac{3}{2} \frac{\delta m}{m} (\beta - z_1 z_2) + x^{1/2} \left[ \delta_1 q \chi_1 (z_2 - \beta z_1) + \frac{\delta_2}{q} \chi_2 (\beta z_2 - z_1) \right. \\
 & + \frac{1}{2} X_1^2 \chi_1^2 (-z_2 - 2\beta z_1 + 3 z_1^2 z_2) + \frac{1}{2} X_2^2 \chi_2^2 (z_1 + 2\beta z_2 - 3 z_1 z_2^2) \\
 & \left. + \frac{3}{2} \eta (\beta - z_1 z_2) (\chi_1 z_1 - \chi_2 z_2) \right] + \frac{3}{2} x \left[ \eta \chi_1 \chi_2 (z_1^2 - z_2^2) \right. \\
 & \left. + X_1^2 \chi_1^2 z_1 (z_1 \beta - z_2) + X_2^2 \chi_2^2 z_2 (z_1 - \beta z_2) \right], \quad (17)
 \end{aligned}$$

where we invoke equations (13) for  $z_1, z_2$  and  $\beta$  to express  $\dot{\gamma}$  in terms of the Cartesian components of  $\mathbf{k}$ ,  $\theta_1, \theta_2, \phi_1$  and  $\phi_2$ . It should be noted that the three Cartesian

components of  $\mathbf{k}$  are provided by equations (6) and therefore the above expression for  $\dot{\gamma}$  depends on  $\theta_1, \theta_2, \phi_1, \phi_2, m, \eta, \chi_1$  and  $\chi_2$  values. We equate such an expression for  $\dot{\gamma}$  to zero and obtain numerically  $\theta_2(x_0)$  value. This approach also allows us to perform the following internal consistency check by obtaining (again) estimates for  $\iota$  and  $\alpha$  at  $x_0$  by using the numerically extracted  $\theta_2(x_0)$  value and equations (6). We generally use the following 2PN-accurate expression for  $L$  at  $x_0$  in the place of  $L_i$  in equations (6) while constructing templates. The 2PN accurate expression for  $|\mathbf{L}|$  in terms of  $x$ , available in [35], reads

$$L_{2\text{PN}}(x_0) = \frac{Gm^2\eta}{c} x^{-1/2} \left\{ 1 + x \left[ \frac{3}{2} + \frac{\eta}{6} \right] + x^2 \left[ \frac{27}{8} - \frac{19\eta}{8} + \frac{\eta^2}{24} \right] \right\}. \quad (18)$$

We are now in a position to compute  $h_{\times,+|Q}(t)$  associated with inspiraling compact binaries that lie in a resonant plane in the aLIGO frequency window. We proceed by computing the Cartesian components of  $\mathbf{s}_1$  and  $\mathbf{s}_2$  at  $x_0$  using the freely specified  $(\theta_1, \phi_1)$  values and the above described  $(\theta_2, \phi_2)$  estimates. The associated Cartesian components of  $\mathbf{k}$  at  $x_0$  arise from equations (6) while invoking the above 2PN-accurate expression for  $|\mathbf{L}|$  in the place of  $L_i$ . These initial conditions are invoked while numerically solving the eleven differential equations, namely equations (7), (8), (15) and (16), to obtain the  $h_{\times,+|Q}(t)$  time-series (we let the initial value of  $\Phi$  to be zero). We terminate these numerical integrations when  $x$  reaches the value  $1/6$  that corresponds to the last stable orbit in the Schwarzschild space-time.

In what follows, certain preliminary data analysis implications of our above inspiral templates for binaries in equilibrium configurations are probed. This is motivated by the possibility of invoking inspiral templates for binaries in the equilibrium configurations to capture GWs from binaries influenced by the spin-orbit resonances. It should be noted that inspiraling binaries in Schnittman's equilibrium spin configurations are characterized by essentially two angular parameters while one requires four angular parameters to fix the initial orientation of the two spins for binaries under the influence of the spin-orbit resonances. This interesting prospect, initially suggested by Schnittman, is probed by computing the match  $\mathcal{M}(s, h)$  involving the expected signal waveforms  $s(t)$  and the employed template waveforms  $h(t)$  [21]. In our  $\mathcal{M}$  computations,  $s(t)$  represents the inspiral GW signal from binaries influenced by the spin-orbit resonance. The template waveforms  $h(t)$ , as expected, model inspiral GWs from binaries in equilibrium configurations as detailed above (we usually employ the expression for  $h_{+|Q}$ , given by equation (14b), to obtain temporally evolving  $s(t)$  and  $h(t)$ ). To obtain  $\mathcal{M}(s, h)$ , we first define the overlap between  $s(t)$  and  $h(t)$  as

$$\mathcal{O}(s, h) = \langle \hat{s}, \hat{h} \rangle = \frac{\langle s|h \rangle}{\sqrt{\langle s|s \rangle \langle h|h \rangle}}, \quad (19)$$

where  $\hat{s}$  and  $\hat{h}$  stand for certain normalized GW signal  $s(t)$  and the associated template  $h(t)$ , respectively. The angular bracket between  $s$  and  $h$  defines certain noise weighted inner product, namely

$$\langle s|h \rangle = 4 \text{Re} \int_{f_{\text{low}}}^{f_{\text{cut}}} \frac{\tilde{s}^*(f) \tilde{h}^*(f)}{S_h(f)} df. \quad (20)$$

In the above equation  $\tilde{s}(f)$  and  $\tilde{h}(f)$  stand for the Fourier transforms of  $s(t)$  and  $h(t)$ , respectively, while  $S_h(f)$  provides the one-sided power spectral density (we invoked

the zero-detuned, high power sensitivity curve of aLIGO [36]). In our computations, the upper cut-off frequency  $f_{\text{cut}}$  is given by  $c^3/(Gm\pi 6^{3/2})$  while we let the lower cut-off frequency  $f_{\text{low}}$  to be 10 Hz. We obtain the match  $\mathcal{M}(s, h)$  by maximizing the  $\mathcal{O}(s, h)$  over the time of arrival  $t_0$  and the associated phase  $\phi_0$ :

$$\mathcal{M} = \max_{t_0, \phi_0} \mathcal{O}(s, h). \quad (21)$$

The results of these match computations are displayed in table 1. The expected inspiral GW waveforms are from the binaries in certain ‘near- and far-resonant’ configurations for four  $\theta_1(x_0)$  values:  $10^\circ, 20^\circ, 35^\circ$  and  $45^\circ$ . The near- and far-resonant configurations have  $\theta_2(x_0)$  values that differ from their equilibrium values by  $\pm 5^\circ$  and  $\pm 20^\circ$ , respectively. The match estimates indicate that the near-resonant configurations tend to have  $\mathcal{M}$  values  $> 0.9$  while these estimates are  $< 0.9$  for far-resonant configurations. Additionally, we list the differences in the accumulated phase ( $\Delta\Phi$ ) in aLIGO frequency window between the resonant, near- and far-resonant configurations. The  $\Delta\Phi$  values, as expected, are large for far-resonant configurations and their match numbers are comparatively lower. The high  $FF$  expectation originates from an investigation that probed the ‘effectualness’ of non-precessing spin templates to capture inspiral GWs from comparable mass precessing binaries [37]. The reported very high  $FFs$  ( $> 0.97$ ) for GWs from a significant fraction of comparable mass precessing binaries were attributed to the fact that the precessional effects are less influential for such binaries. The above 0.97  $FF$  value corresponds to a loss in the event rate not more than 10% of the possible sources within the reach of GW detectors. However, it is rather non-trivial and computationally expensive to pursue similar  $FF$  computations involving inspiral templates for binaries in equilibrium configurations. This is because the procedure involves, in principal, maximization over several binary parameters like  $m, \eta, \chi_1, \chi_2$  and  $\theta_1(x_0)$ . Finally, we note that the listed  $\mathcal{M}$  numbers of table 1 are rather insensitive to the employed differential equation for  $x$ . The changes in the  $\mathcal{M}$  estimates were found to be less than one part in hundred while employing  $dx/dt$  that incorporated all the 3.5PN accurate non-spinning contributions.

**Table 1.** Our estimates for the match and the differences in accumulated phase in the aLIGO frequency window for the BH binaries ( $q = 11/9, m = 30M_\odot$ ) having different values of  $\theta_1$  at  $x_0$ . The second and third columns are for binaries in the near-resonant and far-resonant configurations, respectively. We let the near- and far-resonant configurations to have  $\theta_2(x_0)$  value that are  $\theta_2^R \pm 5^\circ$  and  $\theta_2^R \pm 20^\circ$ , respectively. The  $\Delta\Phi$  (in radians) and  $\mathcal{M}$  estimates associated with the  $\theta_2^R + 5^\circ$  and  $\theta_2^R + 20^\circ$  configurations are shown in the parentheses. The resonant  $\theta_2$  values at  $x_0$ , denoted by  $\theta_2^R$ , are  $21.43^\circ, 41.29^\circ, 66.07^\circ$  and  $79.11^\circ$  for the four  $\theta_1(x_0)$  values and  $\Delta\phi = 0^\circ$  equilibrium configurations. We let  $\phi_1 = 45^\circ$  and  $\Phi(x_0) = 0$ .

$\theta_1(x_0)$	Near-resonance		Far-resonance	
	$\Delta\Phi$	$\mathcal{M}$	$\Delta\Phi$	$\mathcal{M}$
$10^\circ$	0.77 (0.95)	0.988 (0.918)	1.89 (4.80)	0.881 (0.860)
$20^\circ$	1.52 (1.66)	0.963 (0.900)	5.09 (7.32)	0.852 (0.789)
$35^\circ$	2.14 (2.18)	0.910 (0.921)	8.10 (8.76)	0.771 (0.760)
$45^\circ$	2.24 (2.22)	0.926 (0.925)	8.88 (8.53)	0.731 (0.754)

Finally, let us note that it should be possible to construct inspiral templates for binaries residing in the resonant planes while invoking a  $\mathbf{L}_N$ -based non-inertial

triad to specify the initial spins. This will obviously require us to follow what is summarized in section 2.1 to obtain these specific spin configurations in an orbital triad. However, a number of steps are required to evaluate the expressions for  $h_{\times|Q}(t)$  and  $h_{+|Q}(t)$  that require the  $\mathbf{j}_0$ -based inertial frame. In the first step, the three Cartesian components of the total angular momentum at  $x_0$  should be computed. These components define two angles,  $\theta_j$  and  $\phi_j$ , that specify the orientation of  $\mathbf{j}_0$  in the  $\mathbf{L}_N$ -based non-inertial frame. The second step requires us to rotate the  $\mathbf{j}_0$ ,  $\mathbf{L}_N$ ,  $\mathbf{s}_1$  and  $\mathbf{s}_2$  vectors, by the following two angles, namely  $-\theta_j$  and  $-\phi_j$ . This results in a new Cartesian coordinate system where  $\mathbf{j}_0$  points along the  $z$ -axis and  $\mathbf{L}_N$  is specified by  $(\sin\theta_j, 0, \cos\theta_j)$ . This is the frame where one obtains the temporally evolving  $h_{\times|Q}(t)$  and  $h_{+|Q}(t)$  by simultaneously solving the Cartesian components of  $\dot{\mathbf{L}}_N$ ,  $\dot{\mathbf{s}}_1$  and  $\dot{\mathbf{s}}_2$  along with the PN-accurate differential equations for  $\Phi$  and  $x$ . It should be noted that this inertial frame is different from our  $\mathbf{j}_0$ -based inertial frame, depicted in figure 1. This is because the  $x$  and  $y$  axes of these two  $\mathbf{j}_0$ -based inertial frames do not usually coincide. This should be evident from the fact that  $\mathbf{L}_N$  at  $x_0$  is specified only by one angle, namely  $\theta_j$  in the new inertial frame. Therefore, the resulting resonant plane coincides with the plane where both  $\mathbf{N}$  and  $\mathbf{j}_0$  reside. This implies that  $\mathbf{N}$ ,  $\mathbf{j}_0$ ,  $\mathbf{L}_N$ ,  $\mathbf{s}_1$  and  $\mathbf{s}_2$  share a common plane for equilibrium configurations specified in a  $\mathbf{L}_N$ -based orbital triad. Fortunately, the GW phase evolution is not affected by such differences between the two inertial frames.

#### 4. Conclusions

We explored the dynamics of isolated comparable mass spinning compact binaries influenced by Schnittman's post-Newtonian spin-orbit resonances in an inertial frame associated with  $\mathbf{j}_0$ . In contrast, it is customary to describe these special equilibrium configurations in a non-inertial orbital triad [17, 18]. We argued that accurate GW based estimates of the orientations of  $\mathbf{s}_1$ ,  $\mathbf{s}_2$  and  $\mathbf{k}$  from  $\mathbf{j}_0$  at  $x_0$  should allow us to distinguish between the two possible families of spin-orbit resonances. This should be astrophysically interesting as inspiraling binaries, influenced by  $\Delta\phi = 0^\circ$  ( $\Delta\phi = \pm 180^\circ$ ) spin-orbit resonances, are expected to originate from the reverse mass ratio (the standard mass ratio) formation scenarios [19]. Therefore, the accurate measurements of  $\theta'_1, \theta'_2$  and  $\iota'$  should, in principle, allow us to obtain direct observational evidence of possible binary formation channels. The above deductions also apply for binaries that do not remain in a resonant plane when they become detectable by GW interferometers. The resonant plane, characterized by either  $\Delta\phi = 0^\circ$  or  $\Delta\phi = \pm 180^\circ$  restrictions, naturally appears in Schnittman's one parameter family of equilibrium solutions. It turned out that the two black hole spins and the orbital angular momentum usually do not lie in such resonant planes during the later stages of binary inspiral. We emphasized that the accurate GW aided measurements of  $\theta'_1, \theta'_2, \iota'$  and  $\theta_{12}(x_0)$  values will be crucial to distinguish the three possible families of inspiraling comparable mass spinning binaries, namely freely precessing binaries and those influenced by the two types of spin-orbit resonances. We also developed a prescription to compute the time-domain inspiral templates for binaries affected by the spin-orbit resonances. We pursued preliminary data analysis implications of such templates by computing the match estimates. The aLIGO relevant  $\mathcal{M}$  computations invoked inspiral templates for binaries residing in and librating around the equilibrium configurations. The resulting match estimates point to the possibility that a resonant inspiral template bank may provide the acceptable  $FFs \sim 0.97$  for inspiral GWs from

binaries influenced by spin-orbit resonances.

It should be interesting to incorporate the higher order spin-orbit and spin-spin contributions while constructing inspiral templates for binaries in resonant configurations. At present, this is not a straightforward exercise due to the non-availability of next-to-leading order spin-spin contributions to  $dx/dt$ . Note that the next-to-leading order spin-orbit contributions to  $\mathbf{s}_1$ ,  $\mathbf{s}_2$ ,  $\dot{\mathbf{k}}$  and  $\dot{x}$  are indeed available in [35, 38] that are compatible with our equations (7), (8) and (16). In contrast, the next-to-leading order spin-spin contributions to  $\mathbf{s}_1$ ,  $\mathbf{s}_2$  and  $\dot{\mathbf{k}}$  require rather detailed manipulations as the associated orbital dynamics, available in [11], follow different gauge and spin supplementary condition. However, we do not expect that such higher PN order corrections to  $\mathbf{s}_1$ ,  $\mathbf{s}_2$ ,  $\dot{\mathbf{k}}$  and  $\dot{x}$  will influence our estimates for the orientations of  $\mathbf{s}_1$ ,  $\mathbf{s}_2$  and  $\mathbf{k}$  from  $\mathbf{j}_0$  at  $x_0$ . This is because the present description is sufficient to accurately describe the inspiral dynamics of these precessing binaries from  $x_i$  to  $x_0$ . It will also be interesting to compute the accuracies with which we can estimate  $\theta'_1$ ,  $\theta'_2$  and  $\iota'$  values by adapting the detailed analysis presented in [30].

### Acknowledgments

We are grateful to Davide Gerosa, Michael Kesden, Richard O’Shaughnessy and Gerhard Schäfer for helpful discussions and detailed comments.

### Appendix A. Implications of binaries not in spin-orbit resonant configurations

In what follows, we probe the behavior of various dynamical variables for spin configurations that do not force  $\gamma$  and  $\dot{\gamma}$  to be zero at  $x_i$ . It was noted that such configurations usually approach and librate around the equilibrium configurations with steadily decreasing amplitudes during the inspiral as evident from figure 5 in [17]. This prompted Schnittman to suggest that during the inspiral generic spin configurations can approach the equilibrium configurations and eventually get locked into the spin-orbit resonances. The steadily decreasing amplitude of  $\Delta\phi$  oscillations implies that the orbital and spin angular momenta will eventually lie in a plane and this was termed as ‘resonant plane locking’ in [17, 19]. In what follows, we explore the ability of gravitational radiation reaction to force the orbital and spin angular momentum vectors to lie in a plane for binaries influenced by the spin-orbit resonances. This is done by following the evolution of  $\Delta\phi, \gamma$  and  $\dot{\gamma}$  in the  $[10^{-3} - 0.1]$   $x$  interval while choosing  $\theta_1(x_i)$  value to be  $20^\circ$ . The initial  $\theta_2$  values at  $x_i$  differ by  $10^\circ, 20^\circ$  and  $40^\circ$  from the actual resonant value (the resonant  $\theta_2$  value at  $x_i$  being  $173.71^\circ$ ). In figure A1, we display the results of our PN-accurate evolution of these configurations. The plots for  $\Delta\phi$  show that initially these binaries precess freely through a large range in  $\Delta\phi$  and the gravitational radiation reaction forces a substantial reduction in these wild oscillations. However,  $\Delta\phi$  librates about  $\Delta\phi = 0^\circ$  with essentially constant amplitude during the substantial part of the inspiral to  $x_f$  and not with a steadily decreasing amplitude as noted in [17]. Moreover, the plots for  $\gamma$  and  $\dot{\gamma}$  are oscillatory and  $\gamma$  librates around the resonant value, namely  $\gamma = 0$ , with roughly constant and non-negligible amplitudes as these binaries inspiral to  $x_0$ . We have verified that the temporal oscillations in  $\gamma$  and  $\dot{\gamma}$  are such that they do not simultaneously approach zero at any epoch during their inspiral from  $x = 10^{-2}$  to  $x_f$ . Therefore, it is reasonable to infer that the unit vectors along the black hole spins and orbital angular momentum

in these binaries do not lie in a resonant plane, characterized by negligible values of  $\gamma$  and  $\dot{\gamma}$ , when their GWs become detectable by aLIGO.

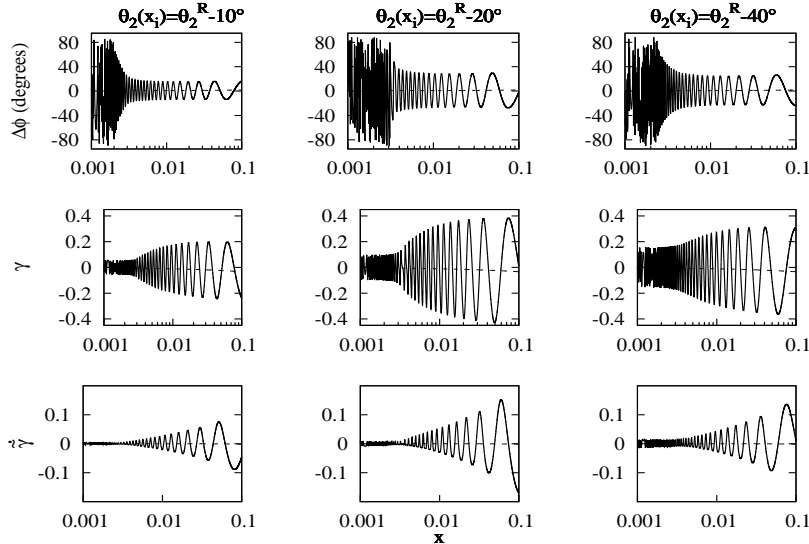


**Figure A1.** Plots of  $\Delta\phi(x)$ ,  $\gamma(x)$  and  $\dot{\gamma}(x)$  for our typical BH binaries initially not in Schnittman’s  $\Delta\phi = 0^\circ$  equilibrium configurations ( $q = 11/9$  and the initial dominant spin orientation  $\theta_1(x_i) = 20^\circ$ ). The three columns are for three different initial  $\theta_2$  values, namely  $\theta_2^R(x_i) - 10^\circ$ ,  $\theta_2^R(x_i) - 20^\circ$ ,  $\theta_2^R(x_i) - 40^\circ$  where the resonant  $\theta_2$  value, namely  $\theta_2^R(x_i) = 173.71^\circ$ . These quantities follow secular evolution for binaries that reside in the  $\Delta\phi = 0^\circ$  resonant plane as shown by the dashed line plots. The non-negligible  $\gamma$  and  $\dot{\gamma}$  evolution indicates that  $\mathbf{k}$ ,  $\mathbf{s}_1$  and  $\mathbf{s}_2$  do not share a plane during the late stages of binary inspiral. These quantities remain essentially unchanged for binaries that reside in the  $\Delta\phi = 0^\circ$  resonant plane (dashed line). The amplitudes of  $\gamma$  and  $\dot{\gamma}$  evolution turned out to be noticeably lower for binaries having  $\theta_1(x_i) \leq 10^\circ$ . This is because such spin configurations are likely to lie in the close neighborhood of another  $(\theta_1, \theta_2)$  equilibrium solution at  $x_i$ .

Let us emphasize that evolution of comparable mass spinning binaries, not in the resonant configurations at  $x = 10^{-3}$ , indeed gets influenced by the spin-orbit resonances and therefore the two spins do not precess freely towards the end of the inspiral. However, such resonances are not very efficient in forcing the two spins and the orbital angular momentum to share a common plane during the late inspiral as evident from the non-negligible values of  $\gamma$  in our figures. We gather from a number of similar numerical experiments that the amplitude of  $\Delta\phi(x)$  oscillations can become small for spin configurations where  $\mathbf{s}_1$  orientations from  $\mathbf{j}_0$  at  $x_i$  are  $< 10^\circ$ . These  $\theta_1(x_i)$  configurations can have multiple  $\theta_2(x_i)$  values that satisfy Schnittman’s  $\Delta\phi = 0^\circ$  equilibrium solution. This is due to the presence of two equilibrium curves at  $r = 1000m$  in the  $(\theta_1, \theta_2)$  plane (see the left panel plots of figure 2). This forces many more  $\theta_2(x_i)$  values, lying in the range  $[0^\circ - 180^\circ]$ , to approach the neighborhood of  $\Delta\phi = 0^\circ$  equilibrium solutions. These configurations turned out to have  $\gamma(x)$  values that are  $< 0.1$  when they inspiral to  $x_0$ .

Finally, we would like to point out that our numerical integrations are fully consistent with those presented in [17, 18, 20]. This is demonstrated by probing the ability of spin-orbit resonances to align the two spins with each other for spin



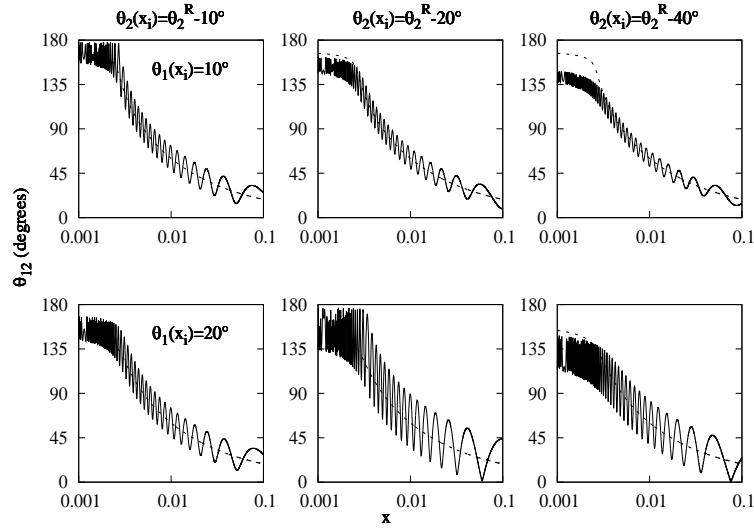


**Figure A2.** Semi-log plots for the  $\theta_{12} = \cos^{-1}(\mathbf{s}_1 \cdot \mathbf{s}_2)$  evolution for binary configurations having  $q = 11/9$ . We consider three non-resonant binary configurations having their  $\theta_2(x_i)$  values differing from their  $\theta_2^R(x_i)$  values by  $10^\circ$ ,  $20^\circ$  and  $40^\circ$ . The two rows are for two different  $\theta_1(x_i)$  values, namely  $\theta_1(x_i) = 10^\circ$  and  $20^\circ$ . The oscillatory nature of the  $\theta_{12}(x)$  plots is consistent with the figure 6 in [17]. The spin-alignment also happens for non-resonant configurations and their  $\theta_{12}$  evolution clearly follow how  $\theta_{12}$  vary for the associated equilibrium solution, depicted by the dotted lines.

configurations lying in the neighborhood of the  $\Delta\phi = 0^\circ$  equilibrium solutions. The spin alignment is clearly visible in the plots of figure A2 where we follow  $\theta_{12}(x)$  evolutions for two initial  $\theta_1$  values that are  $\leq 20^\circ$ . The plots along the two rows are for the two specific  $\theta_1(x_i)$  values, namely  $10^\circ$  and  $20^\circ$  while we vary  $\theta_2(x_i)$  values along the three columns. The chosen  $\theta_2(x_i)$  values differ from their actual resonant values by  $10^\circ$ ,  $20^\circ$  and  $40^\circ$  respectively (the resonant  $\theta_2(x_i)$  values for these two initial  $\theta_1$  values are  $176.75^\circ$  and  $173.72^\circ$ , respectively). We clearly observe substantial reductions in the  $\theta_{12}(x)$  values as these binaries spiral in to  $x_f$  and it essentially leads to the spin-alignment. However,  $\theta_{12}(x)$  evolution is oscillatory as we move away from the equilibrium configurations. The amplitude of  $\theta_{12}(x)$  librations about their equilibrium values depend on both the initial  $\theta_1$  values and the departure of  $\theta_2(x_i)$  from its resonant value. The oscillatory  $\theta_{12}(x)$  evolution is also consistent with the sinusoidal projections in figure 6 of [17]. Therefore, it is reasonable to state that our numerical integrations are consistent with the results of [17, 18].

## References

- [1] Adhikari R X 2013 *Rev. Mod. Phys.* **86** 121 (arXiv:1305.5188)
- [2] Lee K J, Wex N, Kramer M, Stappers B W, Bassa C G, Janssen G H, Karuppusamy R and Smits R 2011 *Mon. Not. R. Astron. Soc.* **414** 3251
- [3] Amaro-Seoane P et al. 2012 *Class. Quantum Grav.* **29** 124016
- [4] Blanchet L, Iyer B R and Joguet B 2002 *Phys. Rev. D* **65** 064005
- [5] Blanchet L, Damour T, Esposito-Farese G and Iyer B R 2004 *Phys. Rev. Lett.* **93** 091101
- [6] Blanchet L, Faye G, Iyer B R and Sinha S, 2008 *Class. Quantum Grav.* **25** 165003

- [7] Jaranowski P and Schäfer G 2012 *Phys. Rev. D* **86** 061503; Jaranowski P and Schaefer G 2013 *Phys. Rev. D* **87** 081503 the references therein.
- [8] Barker B and O'Connell R 1975 *Phys. Rev. D* **12** 329
- [9] Kidder L 1995 *Phys. Rev. D* **52** 821
- [10] Marsat S, Bohe A, Faye G and Blanchet L 2013 *Class. Quantum Grav.* **30** 055007 and the references therein.
- [11] Hartung J, Steinhoff J and Schäfer G 2013 *Annalen Phys.* **525** 359 and the references therein.
- [12] Bohe A, Marsat S and Blanchet L 2013 *Class. Quantum Grav.* **30** 135009
- [13] Arun K G, Buonanno A, Faye G and Ochsner E 2009 *Phys. Rev. D* **79** 104023
- [14] Buonanno A, Faye G and Hinderer T 2013 *Phys. Rev. D* **87** 044009
- [15] Gupta A and Gopakumar A 2014 *Class. Quantum Grav.* **31** 065014, arXiv:1308.1315 [gr-qc]
- [16] Gopakumar A and Schäfer G 2011 *Phys. Rev. D* **84** 124007
- [17] Schnittman J D 2004 *Phys. Rev. D* **70** 124020
- [18] Kesden M, Sperhake U and Berti E 2010 *Phys. Rev. D* **81** 084054
- [19] Gerosa D, Kesden M, Berti E, OShaughnessy R and Sperhake U 2013 *Phys. Rev. D* **87** 104028
- [20] Berti E, Kesden M and Sperhake U 2012 *Phys. Rev. D* **85** 124049
- [21] Damour T, Iyer B R and Sathyaprakash B S 1998 *Phys. Rev. D* **57** 885
- [22] Junker W and Schäfer G 1992 *Mon. Not. R. Astron. Soc.* **254** 146
- [23] Racine E 2008 *Phys. Rev. D* **78** 044021
- [24] Peters P C and Mathews J 1963 *Phys. Rev. D* **131** 435
- [25] Kalogera V 2000 *Astrophys. J.* **541** 319
- [26] Lang R N and Hughes S A 2006 *Phys. Rev. D* **74** 122001
- [27] Klein A, Jetzer P and Sereno M 2009 *Phys. Rev. D* **80** 064027
- [28] Lang R N, Hughes S A and Cornish N J 2011 *Phys. Rev. D* **84** 022002
- [29] Cho H S, Ochsner E, O'Shaughnessy R, Kim C and Lee C H 2013 *Phys. Rev. D* **87** 024004
- [30] O'Shaughnessy R, Farr B, Ochsner E, Cho H S, Raymond V, Kim C and Lee C H 2014 arXiv:1403.0544
- [31] Blanchet L, Damour T, Iyer B R, Will C M and Wiseman A G 1995 *Phys. Rev. Lett.* **74** 3515
- [32] Poisson E 1998 *Phys. Rev. D* **57** 5287
- [33] Mikoczi B, Vasuth M and Gergely L A 2005 *Phys. Rev. D* **71** 124043
- [34] Racine E, Buonanno A and Kidder L E 2009 *Phys. Rev. D* **80** 044010
- [35] Blanchet L, Buonanno A and Faye G 2006 *Phys. Rev. D* **74** 104034
- [36] Abbott B et al. (LIGO Scientific Collaboration) 2010, Advanced LIGO anticipated sensitivity curves, Tech. Rep. LIGO-T0900288-v3
- [37] Ajith P 2011 *Phys. Rev. D* **84** 084037
- [38] Faye G, Blanchet L and Buonanno A 2006 *Phys. Rev. D* **74** 104033